Chem Soc Rev

REVIEW ARTICLE

View Article Online
View Journal | View Issue

Cite this: *Chem. Soc. Rev.*, 2018, **47**, 6370

Silicene, silicene derivatives, and their device applications

Alessandro Molle, [a] Carlo Grazianetti, *[a] Li Tao, *[b] Deepyanti Taneja, [c] Md. Hasibul Alam [c] and Deji Akinwande*[c]

Silicene, the ultimate scaling of a silicon atomic sheet in a buckled honeycomb lattice, represents a monoelemental class of two-dimensional (2D) materials similar to graphene but with unique potential for a host of exotic electronic properties. Nonetheless, there is a lack of experimental studies largely due to the interplay between material degradation and process portability issues. This review highlights the state-of-the-art experimental progress and future opportunities in the synthesis, characterization, stabilization, processing and experimental device examples of monolayer silicene and its derivatives. The electrostatic characteristics of the Ag-removal silicene field-effect transistor exhibit ambipolar charge transport, corroborating with theoretical predictions on Dirac fermions and Dirac cone in the band structure. The electronic structure of silicene is expected to be sensitive to substrate interaction, surface chemistry, and spin–orbit coupling, holding great promise for a variety of novel applications, such as topological bits, quantum sensing, and energy devices. Moreover, the unique allotropic affinity of silicene with single-crystalline bulk silicon suggests a more direct path for the integration with or revolution to ubiquitous semiconductor technology. Both the materials and process aspects of silicene research also provide transferable knowledge to other Xenes like stanene, germanene, phosphorene, and so forth.

Received 28th April 2018

DOI: 10.1039/c8cs00338f

rsc.li/chem-soc-rev

[a] *Consiglio Nazionale delle Ricerche (CNR), Istituto per la Microelettronica e Microsistemi (IMM), unit of Agrate Brianza, via C. Olivetti 2, 20864 Agrate Brianza, MB, Italy. E-mail: carlo.grazianetti@mdm.imm.cnr.it*

[b] *School of Materials Science and Engineering, Southeast University, 2 Southeast University Road, Nanjing, 211189, China. E-mail: tao@seu.edu.cn*

[c] *Microelectronics Research Centre, The University of Texas at Austin, Texas 78758, USA. E-mail: deji@ece.utexas.edu*

Alessandro Molle

Dr Alessandro Molle is a Senior Researcher at the Consiglio Nazionale delle Ricerche (CNR), Istituto per la Microelettronica e Microsistemi (IMM), unit of Agrate Brianza, where he carried out his Post Doc fellowship after PhD and MSc degrees from the University of Genoa, Italy. He has been chairing MSc and PhD courses at the University of Milan-Bicocca and he co-edited a book on two-dimensional (2D) materials for nanoelectronics. He currently is principal investigator of an ERC Consolidator Grant 2017, and previously in charge of other national (Fondazione Cariplo, Regione Lombardia) and international (EU-FP7) grants. His main research interests are on the 2D Xenes and transition metal dichalcogenides.

Carlo Grazianetti

Dr Carlo Grazianetti earned his PhD from the University of Milan-Bicocca in 2014 defending a thesis on the scanning tunneling microscopy investigation of III–V semiconductors and new 2D nanolattices. He is currently a Post Doc fellow working with Dr Molle at the CNR-IMM unit of Agrate Brianza (Italy). His interdisciplinary research expertise covers 2D materials beyond graphene and their applications for nano-electronics and nano-photonics. Since 2011, he has been involved as a key-investigator of molecular beam epitaxy and scanning probe microscopy tasks in EU projects focused on the synthesis and integration into devices of the Xenes (silicene, germanene, stanene, and phosphorene).

1. Silicon at the two-dimensional level

The latest findings in condensed matter physics have witnessed a curious trend, where farsighted theoretical predictions have come to reality sometimes with unexpected turns. Although, on one hand, for instance, the isolation of graphene clearly contradicted the well-established Mermim's theorem,[1] conversely, on the other hand, the rise of topology as a physical (and not only mathematical) concept to interpret the new solid state phases, *e.g.* topological insulators (TIs),[2] is the most astonishing example to prove that theory is often able to see further on yet to be realized materials. Notably, the initial theoretical investigation subsequently resulted in extensive experimental efforts. Quite similarly, it can happen that due to the periodic table kinship, one may wonder why there would not exist two-dimensional (2D) honeycomb lattices made of silicon, germanium, or tin, as they are placed just below carbon and, like a gedanken experiment, conceive a brand new material. This is what occurred in 1994 when Takeda and Shiraishi proposed the aromatic stages of silicon and germanium. Indeed, as they wrote in their pioneering work, ''the present infinite 2D Si aromatic stage (*i.e.* silicene) is a hypothetical material, but it is an important model for investigating the aromaticity of Si elements''.[3] In this humble way and perhaps with a modest purpose, the concept of silicene made its debut as a 2D honeycomb lattice of

Li Tao

Dr Li Tao is a Young 1000-Talent Awarded Professor in the School of Materials Science and Engineering at Southeast University. Prior to 2016, he was a research scientist at the Microelectronics Research Center, the University of Texas Austin. He received his PhD from the University of Texas Dallas in 2010 with an inventor recognition award. His research expertise cover 2D materials and flexible micro/nano electronics, nanofabrication and nanomedicine, with research featured in the TIME blog and 50+ tech media. He serves as a committee member for the EIPBN (3-beam) conference, young associate editor for Chinese Chemical Letters, board member for MRS China young scientist branch and panel reviewer for NSF China.

Deepyanti Taneja

Dr Deepyanti Taneja is a Post Doc fellow working with Prof. Akinwande at the Microelectronics Research Center, University of Texas at Austin. She received her PhD in 2016 in semiconductor physics from the University of Cambridge, UK, where she was a member of St. Catharine's College. Her doctoral research focussed on the development and low temperature measurement of novel low-dimensional devices based on undoped GaAs/AlGaAs heterostructures. Prior to this, she pursued her master's degree in physics at University College London and bachelor's degree at Hindu College, University of Delhi. Her current research interests lie in device development and engineering of 2D Xenes and transition metal dichalcogenides.

Md. Hasibul Alam

Md Hasibul Alam is a graduate student at The University of Texas at Austin working towards his PhD degree under the supervision of Prof. Akinwande. He started his PhD in Fall 2015 and is currently working on process development for device fabrication and characterization of transistors based on 2D Xenes. He completed his MSc (2014) and BSc (2012) in Electrical and Electronic Engineering (EEE) from Bangladesh University of Engineering and Technology (BUET). During his MSc, he did extensive simulation on the structure, electronic and transport properties of 2D materials and III–V material-based heterostructures.

Deji Akinwande

Dr Deji Akinwande is an Endowed Faculty Fellow and Associate Professor at the University of Texas at Austin. He received a PhD from Stanford University in 2009. He has been honored with the 2017 Bessel-Humboldt Research Award, the U.S Presidential PECASE award, the inaugural Gordon Moore Inventor Fellow award, the inaugural IEEE Nano Geim and Novoselov Graphene Prize, the IEEE ''Early Career Award'' in Nanotechnology, the NSF CAREER award, and several DoD Young Investigator awards, and is a past recipient of fellowships from the Kilby/TI, Ford Foundation, Alfred P. Sloan Foundation, 3M, and Stanford DARE Initiative. He serves as an Editor for IEEE and Springer-Nature. He is a Fellow of the American Physical Society (APS).

silicon atoms even earlier than the rise of graphene in 2004.[4] More recently, silicene has attracted substantial interest as a material for nanotechnology owing to its unique solid-state properties including the quantum spin Hall (QSH) effect (a 2D TI state), strong spin–orbit coupling (SOC), giant magnetoresistance, field-tunable bandgap, non-linear electro-optic effects, and piezo-magnetism.[5–11] Silicene can be considered a prototype of the elemental analogues of graphene, including germanene, stanene, *etc.* referred to as Xenes.[12] Importantly, Xenes feature a non-planar atomic structure, which enhances certain physical properties such as the SOC, out-of-plane phonon scattering and other related physics. However, the metastable silicene structure also results in generally poor air-stability that can be addressed by proper encapsulation or passivation of reactive surfaces. The latter aspect paves the way for designing 2D materials with passivated surfaces due to functionalization, including hydrogenation which is predicted to both stabilize silicene (similar to the passivation of bulk silicon)[13] and also boost its bandgap while maintaining the atomically-thin profile.[14,15]

In this light, a major driver for silicene (and generally Xenes) research is the potential device benefits from ultra-scaled silicon technology for conventional, flexible, and quantum or topology-based information processing. Silicon has been at the heart of complementary metal-oxide semiconductor (CMOS) technology for over five decades, especially because of the lucky combination with its oxide establishing the probably most studied interface ever.[16] With Moore's law as the driving engine (namely, the temporal expansion of the number of transistors in a chip), significant performance and cost-related gains have been achieved from one technology node to the next, as the lateral size of the semiconductor devices is reduced along with the scaling of the silicon channel thickness.[17] More specifically, an order of magnitude reduction in the silicon channel thickness has resulted in approximately an order of magnitude power reduction in continuously scaled devices thus promising a solid advance in device miniaturization and densification in a chip. However, the conventional Smart-Cut approach (*i.e.* a top-down technology for the transfer of a thin layer of silicon from a donor substrate to another substrate, mainly used for silicon-on-insulator wafer manufacturing) to produce an ultra-thin silicon body, suffers from an intrinsic physical limitation for scaling beyond 5 nm.[18] On the other hand, starting from a bottom-up approach, it is possible to synthesize 2D mono-elemental sheets of silicon, resulting in the ultimate thickness scaling and the associated reduction in electronic device power consumption. Moreover, while the carrier mobility deteriorates with scaling in the traditional ultrathin body silicon, this is not the case with silicene or 2D silicon.[19,20] 2D silicon can also be stacked vertically enabling three-dimensional integrated chips in a layer-by-layer fashion.

In addition to its conventional semiconducting properties, certain epitaxial phases of silicene that feature the QSH effect can be employed for making topological devices such as a gate-controlled topological field-effect transistor (FET) that is based on topological phase change.[12] However, for all the novel concepts based on Xenes to be realized for applications, the air-stability issue and process integration onto technologically relevant substrates will have to be decisively tackled. In this review, our intent is to briefly retrace the silicene thread by providing an overview of the chemistry and physics of silicene, including the most relevant experimental achievements in terms of synthesis and chemical functionalization (Section 2), methodologies for silicene processing (Section 3), and for silicene integration into nanotechnology platforms (Section 4).

2. Epitaxial silicene

2.1 Chemistry and physics of silicene

The theoretical background of silicene and germanene dates back to the seminal paper by Takeda and Shiraishi on the hexagonal rings of silicon and germanium with reference to the carbon counterpart.[3] These aromatic stages were predicted to be more stable in a regularly corrugated structure (so-called buckled with a D_{3d} group symmetry) compared with the flat state (D_{6h} group symmetry) stage that is specific to carbon. This picture was then confirmed by total energy minimization *ab initio* calculations.[21] This intrinsic puckering, hereafter referred to as buckling, is the origin of many peculiar properties (Fig. 1a). The mirror symmetry breaking in silicene by buckling removes the instability associated with the planar high-symmetry structure. Buckling arises from the pseudo Jahn–Teller distortion associated with the coupling between occupied and unoccupied molecular orbitals where σ–π orbital mixing allows the system to gain stability.[22] It is noteworthy, conversely, that the low buckling does not break the hexagonal symmetry, *i.e.* for the honeycomb lattice the two atoms in the unit cell are equivalent and electrons can hop among the

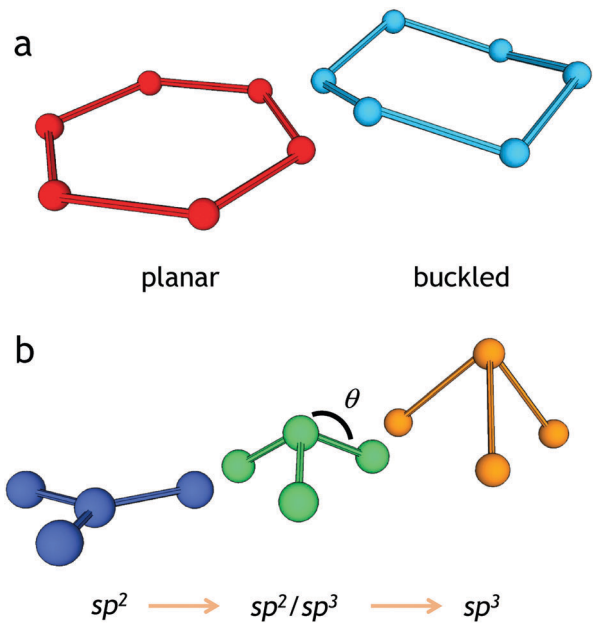

Fig. 1 Chemical bonds in silicene. (a) Planar and buckled hexagonal ring stages, (b) evolution from sp^2 to sp^3 hybridization of the four-bonded group 14 Xenes.

nearest-neighbour atoms, thus retaining the existence of Dirac fermions.[23] In this framework, the Si–Si bond length in the buckled state (2.247 Å) is longer than the flat stage (2.226 Å), thereby resulting in a larger effective volume of the lattice unit size.[3,22] Nonetheless, electrons in the buckled state are more delocalized (in and out of the stage plane) producing a smaller inter-electron repulsive energy. This deformation also causes a partial sp^3 hybridization, which is the second marked difference with respect to graphene. While silicon prefers sp^3 hybridization in its bulk form, the interplay between sp^3 and sp^2 hybrid bonds is characteristic of silicene (Fig. 1b). The mixed sp^2–sp^3 hybridization state can be understood as evolving with the buckling and, more specifically, with the θ angle, *i.e.* the angle between the Si–Si bond and the direction normal to the plane. Hence, the sp^2 (planar), low-buckled (mixed sp^2–sp^3), and sp^3 configurations correspond to $\theta = 90^\circ$, $\theta = 101.73^\circ$, and $\theta = 109.47^\circ$, respectively (Fig. 1b).[5] Despite the stability issues that may arise from unsaturated sp^3 bonding, buckling represents an additional degree of freedom to manipulate the silicene properties such as bandgap opening, electronic structure, incorporated staggered field, and selective chemical reactivity. On the other hand, buckling exposes silicene to have mixed sp^2 and sp^3 hybrid bonds, which results in a high environmental reactivity eventually leading to material degradation (see Sections 3.1 and 3.2).

In terms of the electronic band structure, buckled silicene appears as a graphene-like Dirac crystal where π and π^* bands cross linearly at the Dirac points, namely high symmetry K and K' points in the hexagonal Brillouin zone.[21,24,25] Additional theoretical efforts on the freestanding silicene have focused on its optical and topological properties. Indeed, similar to graphene, the low-frequency absorbance of freestanding silicene and other Xenes is basically determined by the fine-structure constant (or Sommerfeld's constant) $\alpha = e^2/\hbar c$ (e, $\hbar$, and c being the electron charge, the reduced Planck constant, and the speed of light, respectively), irrespective of the X atom or the buckling character of its bonds, whereas differences occur at higher frequencies due to interband transitions related to the van Hove singularities of the joint density of states (DOS).[26] On the other hand, when the lattice gains weight from the (planar) graphene to (buckled) Xenes for X spanning from silicon to tin, a topologically nontrivial electronic structure sets in due to the increasing SOC, which results in the QSH effect, namely the physical hallmark of a 2D TI phase of matter.[5,9,25,27] Based on the Kane–Mele model,[28] the effective SOC in the buckled Xenes opens a gap at the Dirac points that is topological in character, and hence endowed with conductive edge states at the geometrical borders, *e.g.* at the boundaries of a silicene ribbon. Furthermore, the stronger the effective SOC is at the Dirac points, the larger the gap opening is. That is why topological properties are expected to be more robust in Xenes with increasing atomic mass such as germanene and stanene.[12] In this scenario, an even richer topological phase diagram can be envisaged which includes quantum anomalous Hall effect states, valley-polarized metal phases, and chiral superconducting states as a function of an externally applied electromagnetic field or an intrinsic exchange field.[5,12,29–31]

Driven by this perspective, the recently developed paradigm of epitaxial silicene on a substrate has been extended to other Xenes[12,32] with a nearly silicene-like approach to the synthesis and identification. In this respect, increasing theoretical and experimental effort has been recently devoted to template engineering, namely designer weakly or non-interacting substrates serving as templates for silicene. Promising substrates of this kind include insulators,[33] semiconductors,[34–38] and metals.[39]

2.2 Main achievements in the synthesis of silicene

Due to the absence of a graphite-like form of silicon in nature, silicene as well as all the Xenes, is synthesized by means of a bottom-up approach, namely epitaxial growth on a substrate. Despite the relatively high cost, this approach offers potential wafer scale production targeting technology applications. Physical identification of silicene (and Xenes) usually relies on the interplay between an experimental tool such as scanning tunnelling microscopy/spectroscopy (STM/S) or angle-resolved photoelectron spectroscopy (ARPES), and density functional theory (DFT) calculations. Three general routes have been implemented for the silicene epitaxy so far (see Fig. 2): (a) thermal evaporation on a substrate (epitaxial silicene by deposition); (b) surface segregation from a substrate (epitaxial silicene by segregation); (c) intercalation through a silicide network (intercalated silicene).

(a) Epitaxial silicene by deposition. The process stems from the condensation and self-organization of thermally evaporated silicon atoms onto a substrate (Fig. 2a). Although the number of substrates on which silicene can be synthesized is rapidly expanding, the (111)-terminated silver substrate is the only one enabling both the synthesis and device integration as yet. In this respect, it is important to note that while Ag(110) was originally shown to accommodate silicon nanoribbons with a hexagonal[40] or pentagonal[41] structure, Ag(111) has proven to be a quite universal template for other Xenes such as borophene,[42,43] germanene,[44] stanene,[45] and antimonene.[46] Moreover, the Ag(111) template can be suitably reduced to an epitaxial film on mica or Si(111)[47] substrates, thus avoiding the unpractical use of highly expensive monocrystalline silver substrates and enabling delamination in subsequent processing (see Section 3). Lattice commensuration with the freestanding form of silicene and a narrow growth parametric window (mostly temperature and deposition flux) are the key pre-requisites of the sought-after recipe for the synthesis of silicene on Ag(111) by epitaxial deposition.[48,49] This methodology has been successfully replicated on other substrates, including iridium,[50] molybdenum disulphide (MoS_2),[51] zirconium carbide (ZrC),[52] ruthenium,[53] and graphite.[54] In most cases, epitaxial silicene by deposition takes place on a large-scale through the emergence of differently reconstructed domains. Reconstructions arise as lattice-distortion of the freestanding silicene driven by the commensurability relationship with the surface lattice of the substrate.[55–58] Based on STM investigations,

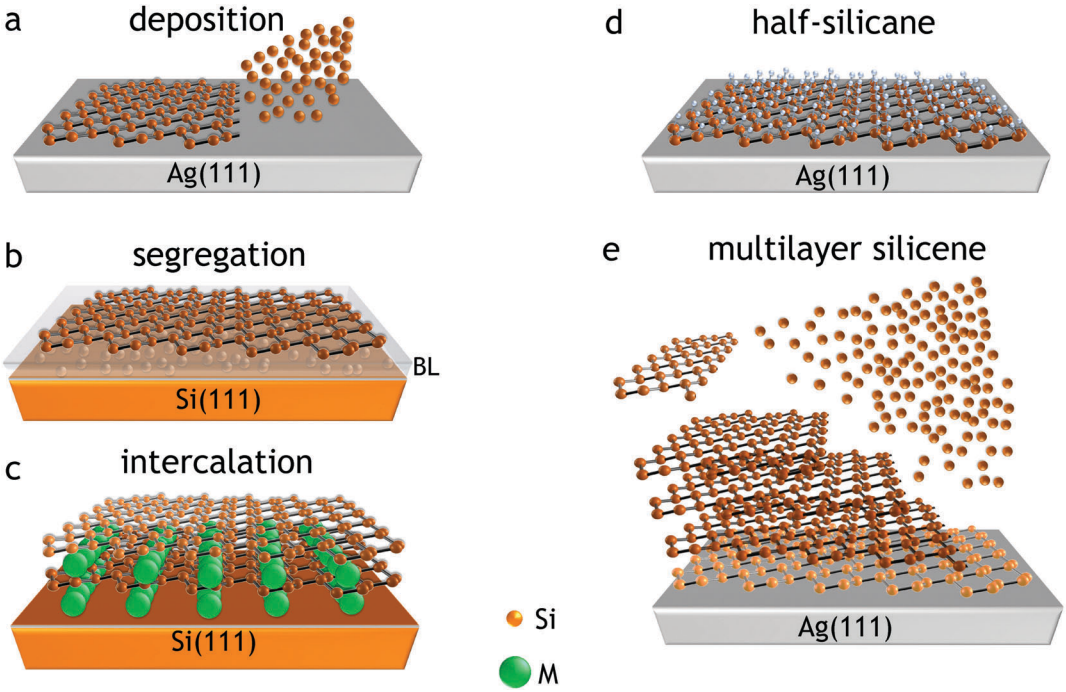

Fig. 2 Silicene growth methodologies. (a) Epitaxial silicene by deposition where the hot incoming atoms are condensated onto a supporting template: the case of epitaxial silicene on Ag(111).[48] (b) Epitaxial silicene by segregation where the supporting substrate acts as a reservoir through a buffer layer: the case of epitaxial silicene on ZrB_2 as a buffer layer grown on Si(111),[75] (c) intercalated silicene where foreign atoms are intercalated in a pre-established network: M (Eu, Sr, or Gd) atoms are supplied by a film pre-grown on a Si(111) substrate and then intercalated through a layered silicide network;[81–83] (d) functionalization of silicene exemplified in the half-silicane after H_2 exposure to Ag(111)-supported silicene;[103] (e) silicene multilayer by deposition on a Ag(111) susbtrate.[108]

specifically on Ag(111)-supported silicene, periodic reconstructions mainly include 4×4, $\sqrt{13} \times \sqrt{13}$, and $2\sqrt{3} \times 2\sqrt{3}$ surface phases (terminologies refer to the coincidence of the silicon atoms with respect to the surface atoms of the substrate, see Fig. 3a) of the epitaxial silicene as opposed to the alternating sequence of up and down adjacent atoms in freestanding silicene, namely a 1×1 phase. As such, the buckling distribution, *i.e.* the periodic arrangement of non-planar buckled bonds in each surface phase, and hence, the Si–Si bond length can vary from one superstructure to another. In the case of the Ag-supported silicene, a comprehensive phase diagram can be sketched up as a function of the substrate temperature and silicon coverage.[56–61] To complement STM studies, ARPES provides evidence of the electronic band structure of silicene. In these kinds of studies, some interference is produced by the inevitable orbital interaction of silicene with the substrate, which makes the silicene metallic in character.[62,63] As such, isolation of the true characteristics of silicene when it is supported on silver is made difficult by the bandfolding of the silicene reconstructions and the linear dispersion of silver bands near the Fermi level.[62–73] The case of Ag-supported silicene is then qualified by the suppression of the π molecular orbitals as a consequence of the hybridization of the silicon and silver electronic states, whereas the σ orbitals are clearly identified.[65] Nonetheless, evidence of a low-energy plasmonic excitation was recently deduced from electron energy loss spectroscopy, and it is consistent with characteristic π-like plasmons in freestanding silicene.[74]

(b) Epitaxial silicene by segregation. In this configuration, the reservoir of silicon atoms is supplied by the underlying substrate instead of the deposition flux (Fig. 2b). An example in this respect is the case of the silicon atoms thermally diffusing from a (111)-terminated silicon substrate up to the surface of a thin crystalline zirconium diboride (ZrB_2) film.[75] Similar to the epitaxial silicene by deposition, the self-organization of the silicene lattice is dictated by the commensurability with the ZrB_2 surface lattice. Interaction with the substrate determines the electronic band structure of the overall surface system but in contrast to the metallicity of the metal-supported silicene, the ZrB_2-supported silicene results in a gapped electronic structure.

(c) Intercalated silicene. Complementary to the physical deposition techniques usually adopted in the silicene framework, the synthesis of silicon nanosheets can be carried out *via* chemical methods. The chemistry versatility allows for synthesizing silicon nanoparticles/dots, silicon fullerenes, silicon nanowires, silicon nanotubes, and silicon nanoribbons (for details see ref. 76 and references therein). A paradigmatic example is represented by silicon nanosheets naturally embedded in calcium disilicide ($CaSi_2$).[77,78] The idea here is to find pre-formed silicene-like structures to be synthesized *via* topochemical deintercalation of the silicide.[79] $CaSi_2$ is a Zintl silicide, where 2D silicon puckered sheets made of Si_6 rings are separated from each other by planar monolayers of Ca^{2+},[80] *i.e.* intercalated multilayer silicene. Chemical manipulation through fluoride

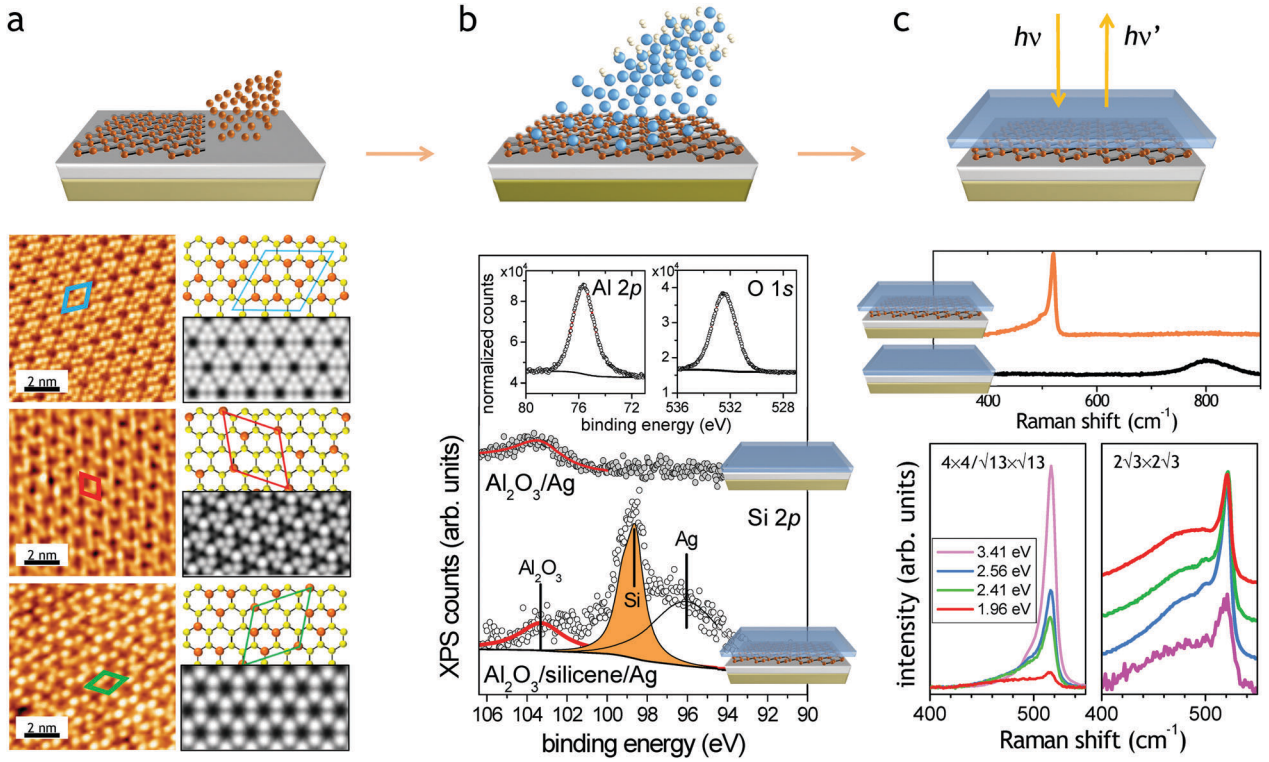

Fig. 3 Route for silicene encapsulation. (a) Epitaxial growth of silicene on Ag(111)/mica substrates. The three different silicene phases (4×4, $\sqrt{13} \times \sqrt{13}$, and $2\sqrt{3} \times 2\sqrt{3}$, from top to bottom) are identified by high-resolution STM (left side), explained in terms of atomic lattice sketches (right side, top) where the yellow and orange spheres correspond to the lower and upper atoms, respectively, rhombi highlight the unit cells, and match with the respective DFT simulations. DFT simulations of STM images are adapted from ref. 180 with permission from IOP publishing, copyright 2012. (b) Encapsulation by means of reactive co-deposition of Al and O_2. Probing the Si 2p core-level (bottom spectra) in the silicene-free control Al_2O_3/Ag structure and in the Al_2O_3/silicene/Ag stacked structure shows evidence of the integrity of the elemental silicon bonding (orange peak) retained in the encapsulated silicene (left side feature at a higher binding energy is assigned to the Al_2O_3 background after comparing the two reported structures); formation of a stoichiometric Al_2O_3 capping layer is confirmed by the observation of the Al 2p and O 1s core-level lines (top spectra). Data are adapted from ref. 141 with permission from John Wiley and Sons, copyright 2013. (c) Raman spectroscopy (excitation energy: 2.41 eV) of encapsulated silicene. Raman spectra are acquired with and without silicene in between an Ag-on-mica substrate and the Al_2O_3 capping layer (top panel); when silicene is in, a well-defined peak is measured as a characteristic signature. The multi-wavelength (excitation laser energies from the ultra-violet down to the visible blue, green, and red are listed in the legend) Raman spectroscopy study (bottom panel) shows a resonant and non-resonant behaviour for the encapsulated $4 \times 4/\sqrt{13} \times \sqrt{13}$ (left) and $2\sqrt{3} \times 2\sqrt{3}$ (right) phases, respectively. Adapted from ref. 148 with permission from the American Chemical Society, copyright 2013.

diffusion into $CaSi_2$ results in the formation of silicon layered structures in between calcium fluoride (CaF_2) planes with a reduced number of unsaturated silicon bonds and bandgap opening.[78] Starting from a similar framework, Tokmachev *et al.* have reported on the *ad hoc* tailored silicidation where silicon atoms from a bulk substrate are thermally intercalated through epitaxially deposited strontium, europium, or gadolinium so as to form Zintl phase silicide (*e.g.* $SrSi_2$, $EuSi_2$, $GdSi_2$) where silicene nanosheets are incorporated as network constituents (see Fig. 2c).[81–83]

Although the quest for silicene still justifies the search for a special and easy route of its reliable synthesis, other silicon-based nanostructures have been recently investigated as well. Indeed, every kind of nanoscaled silicon compatible with the electronics industry represents a possible solution to replace cubic silicon in scalable devices and fulfil the technology scope as outlined in Section 1. In this framework, theoretical efforts were mainly driven to explore the allotropic phases of silicon other than silicene,[84–86] whereas the experimental activity successfully provided evidence of hexagonal silicon, the so called lonsdaleite phase,[87] or the new orthorhombic allotrope of silicon called Si_{24}.[88] Another flourishing field is related to the low-dimensional silicon nanosheets that are endowed with unconventional properties. Within this latter class, the generic term of silicon nanosheets refers to silicon nanomaterials and nanostructures, which exhibit properties different from those of bulk silicon due to the quantum confinement effects.[76] For instance, cubic silicon nanosheets in the thickness range of 1–13 nm display strong thickness-dependent photoluminescence in the visible range with the bandgap energies ranging from 1.6 to 3.2 eV.[89] In nearly the same thickness range (2–18 nm), the excitation energy-dependent Raman intensity of ultrathin silicon nanomembranes relies on the combined effects of interference and resonance from the band structure modulation.[90]

Apart from the epitaxial methods, chemical processing is rapidly emerging as a route to achieve large-scale and low-cost production of silicon nanosheets with a thickness of ~4 nm

and a lateral size of several micrometres. In this respect, Lang *et al.* developed a scalable synthesis of ultra-low friction silicon nanosheets by means of the intrinsic delithiation process of the $Li_{13}Si_4$ alloy that possesses an orthorhombic structure markedly different from that of $CaSi_2$.[91]

2.3 Silicene derivatives and functionalization

Two main follow-up topics tail the epitaxial synthesis of silicene: chemical functionalization and pile-up stacking of multi-layered silicene. Both routes are conceived to take the silicene single layer as a precursor for a new artificial material with expanded functionalities. In the former aspect, a number of theoretical studies have conceptualized the absorption of foreign chemical atoms/molecules to yield functionalized silicene,[92–97] but the experimental activity has been mainly focused on oxygen and hydrogen functionalization thus far. Oxidation is probably the easiest route to modify the silicene bandgap.[98] Silicene can be exploited as the precursor stage for silicene oxides,[99,100] alternative to hexagonal boron nitride (hex-BN) and in parallel with the current effort to synthesize 2D honeycomb-like silica.[101] Interestingly, oxygen intercalation allowed the formation of a freestanding-like silicene.[102] The oxygen atoms intercalate into a bilayer silicene on the Ag(111) surface, resulting in the isolation of the top layer of silicene. This layer exhibits the signature of a 1×1 honeycomb lattice and hosts massless Dirac fermions due to the weaker interaction with the substrate, similar to the intercalation approach described in Section 2.2. Hydrogen absorption into silicene is also appealing as a molecular dissociation path for the hydrogen evolution reaction.[103] As full hydrogenation is inhibited by the substrate at the bottom surface, the final product is the half-silicane, *i.e.* just the top surface undergoes hydrogenation therein showing an asymmetric out-of-plane structural configuration[103,104] (see Fig. 2d for a pictorial sketch for half-silicane). Interestingly, the silicene hydrogenation process has been demonstrated to be reversible.[105]

Retracing the route of silicene's synthesis, one may wonder whether graphite-like silicon can be artificially created by piling up single layers of silicene. Such a crystal, termed silicite, was predicted to set in as a new thermodynamically stable layered-phase of silicon, characterized by stacking of dumbbell patterned silicene sheets with strong directionality in the electronic and structural properties.[106,107] Additionally, the increased absorption in the visible range would make silicite,[106] as well as other allotropic silicon phases[84,88] very interesting for silicon-based photonics. Experimentally, multilayer silicene is referred to as the sequential deposition of individual silicene layers by epitaxy starting from the first one as a template (see Fig. 2e for a pictorial sketch for multilayer silicene). The as-defined multilayer silicene on Ag(111) shows an island growth mode with a characteristic termination, which is independent of the number of layers (≥ 2).[108–111] Similar to the single-layer silicene, the presence of Dirac fermions and the layered nature of this artificial crystal are highly debated in the literature[111–113] and the true character of the surface termination (being made of silicon or segregated silver from the substrate) is still controversial.[114–116] Nonetheless, increasing the growth temperature was proven to govern the transition from the as-defined multilayer silicene to cubic silicon.[117] Although the multilayer silicene on Ag(111) is yet to be fully understood, we emphasize the role played by the seed single layer silicene in determining its structural and electronic properties.[117] For this reason, multilayer silicene can be regarded as a derivative of silicene. As alternative to the epitaxy, multilayer silicene growth has been also reported by ion implantation.[118]

2.4 The class of epitaxial Xenes

The route of silver templating not only drove the epitaxial synthesis of silicene but also inspired an intense effort to synthesize similar materials made of elements other than silicon. These are the epitaxial Xenes. The term Xenes, originally restricted to group 14 elements,[12] is being gradually expanded to include the ever-growing class of 2D monoelemental crystals spanning from group 13 to 16 of the periodic table. Experimentally realized Xenes, today, stretch out from the 2D icosagens (from group 13 elements) like borophene[42,43] and the recently reported gallenene,[119] sought-after, to 2D pnictogens (*e.g.* phosphorene, antimonene, and bismuthene)[120,121] and 2D chalcogens (selenene, tellurene).[122] Leveraging on the advances from synthesizing silicene, molecular beam epitaxy is gaining the largest popularity, mainly because of its ability to offer atomic-scale precision. Therefore, we focus on Xenes grown by epitaxy in this section. Experimental facts for Xene identification are generally based on STM/S and ARPES investigation supported by DFT models. Epitaxial growth was successfully applied to the following groups of elements in the periodic table:

– Group 13 (icosagens): borophene was demonstrated independently by two groups on the Ag(111) surface[42,43] providing evidence of two different unbuckled phases with a metallic nature;

– Group 14: growth of metallic germanene has been demonstrated on several metallic (111)-terminated surfaces (so far including aluminium, copper, gold, platinum, antimony),[123–127] and a limited number of non-metallic substrates [MoS_2 and hexagonal aluminium nitride (hex-AlN)],[128,129] being of metallic character in both cases; evidence of epitaxial stanene is limited to substrates where stanene originates from a single-layer of the α-tin phase, such as bismuth telluride (Bi_2Te_3)[109] and InSb(111),[130] or as a second layer on top of the Ag(111) surface;[45]

– Group 15 (pnictogens): the monolayer of hexagonal phosphorus, namely phosphorene (also termed blue phosphorus),[131] was reported on the Au(111) surface[132] with a semiconducting character (gap of 1.12 eV from the local density of states) and a silicene-like buckled structure (as opposed to the more stable black phosphorus);[132] other epitaxially grown 2D pnictogens in this category include bismuthene on Bi_2Te_3[133] and silicon carbide (SiC)[134] substrates, and antimonene on germanium, palladium telluride ($PdTe_2$), and silver substrates.[46,135,136]

– Group 16 (chalcogens): this is the case of van der Waals (vdW) epitaxy of 2D tellurium, termed tellurene, on highly oriented pyrolytic graphite (HOPG)[137] and graphene/6H-SiC substrates,[138] and 2D selenium, termed selenene, on a freshly

cleaned Si(111) substrate.[139] Unlike previously mentioned Xenes, the case of tellurene and selenene differs in that they are inherently made of an array of parallel atomic chains arranged on a 2D hexagonal framework. As such, they are referred to as a one-dimensional vdW crystal.[140]

Aiming at a universal approach to device fabrication (see Section 3.5), it deserves to be noted that most of the epitaxial Xenes listed above are hosted by (111)-terminated silver or gold templates that in turn bear epitaxy on cleavable mica substrates. As such, they tend to be treated by delamination in a subsequent processing stage as detailed in Section 3.

3. Silicene processing

3.1 The route to silicene devices: interface engineering

The oxidation of silicene is quite limited when exposed to pure molecular oxygen (O_2) under ultra-high vacuum (UHV) conditions,[141,142] but its unavoidable degradation under ambient conditions is widely reported.[100,143,144] Even though the exact oxidation mechanisms deserve further insights (see Section 2.3), the extreme surface sensitivity of silicene, arising from its metastable nature, requires strategic interface engineering to preserve its properties right from its synthesis, all the way down to device fabrication and post-fabrication characterization. There are three technical milestones, all related to strategic interface engineering, in silicene processing towards a functional device. The first milestone is the synthesis of silicene on cleavable Ag(111)/mica substrates with *in situ* STM and *ex situ* Raman spectroscopy as front-end characterization (Fig. 3). The second milestone is the design of the aluminium oxide (Al_2O_3)/silicene interface with Al_2O_3 as a capping layer to preserve silicene when exposed to post-deposition under ambient conditions. As seen in Section 3.2, these two advances addressed the accessibility issues (large-scale silicene sheet with affordable separation process from growth substrate) and stability issues (pristine silicene after deposition but before transfer or decoupling from growth substrates to a device substrate) in silicene processing. The latest milestone is the design of the transfer and device fabrication process with the top and bottom interfaces of silicene sandwiched in between a capping Al_2O_3 layer[141] and the underlying growth catalyst Ag(111), known as silicene encapsulated delamination with the native electrode (SEDNE) process.[145] The SEDNE process (details and development in Section 3.3) addressed both stability and portability (intact silicene during transfer/decoupling and device fabrication) issues. These two aspects share a common cause: silicene is a metastable phase originating from its mixed sp^2–sp^3 silicon sheet (see Section 1.2).

3.2 Encapsulation and Raman spectroscopy of silicene

Here we will focus on the key enabling technologies for accessibility and stability of silicene. Accessibility of a silicene sheet was enabled by the successful use of a cleavable mica substrate as a host for the Ag-supported silicene (Fig. 3a). This is basically due to the fact that mica can epitaxially accommodate the Ag(111) film with high structural quality. Based on STM investigations in Fig. 3a, silicene phases as detailed in Section 2.2 can be nicely reproduced on an epi-Ag(111) film supported by mica with the extra-value of being cleavable from the background substrate compared to conventionally used (111)-terminated silver monocrystals. On the other hand, the handling of silicene is hindered by the stability of the top (exposed) surface while the bottom one is protected by the interface with the silver catalyst substrate. Stabilization of the Ag-supported silicene was first reported by means of *in situ* encapsulation with an ultra-thin (few nm) Al_2O_3 layer. Al_2O_3 is sequentially grown after silicene by means of reactive co-deposition of an aluminium flux in O_2 rich pressure (partial pressure 1×10^{-6} mbar) at room temperature in an UHV background environment (Fig. 3b).[141] Chemical evidence of stoichiometric Al_2O_3 as well as silicene integrity after co-deposition is given by *in situ* X-ray photoemission spectroscopy (XPS) that rules out any intermixing or compound formation involving silicene. A sketch of the Al_2O_3 encapsulation process and the related XPS survey are illustrated in Fig. 3b. The same methodology has been successfully implemented in highly-buckled silicene grown on MoS_2 where the chemical integrity of the silicon nanosheet is again demonstrated by *in situ* XPS.[146] This is not the case of the silicene grown on ZrB_2 where dissociative chemisorption is observed to take place in between silicon and O_2 thus resulting in an Al-mediated oxidation of the ZrB_2-supported silicene; AlN is therein proposed as an alternative solution bypassing the silicene oxidation.[147] Nonetheless, the effectiveness of the Al_2O_3 capping layer on the Ag-supported silicene has been validated by the observation of a characteristic Raman spectrum of silicene,[148] as discussed in the following. Raman spectroscopy offers a quick and effective identification tool that is conventionally used to characterize graphene (and in general, carbon-based nanosystems) and other 2D layered materials in terms of the atomic structure, disorder, defects, and electronic properties.[149] Despite the presence of the metal substrate (that is intrinsically Raman silent), the Raman spectrum of the Ag-supported silicene exhibits an intense peak located at 516 cm^{-1} (for the 4×4 and $\sqrt{13} \times \sqrt{13}$ phases) or 521 cm^{-1} (for the $2\sqrt{3} \times 2\sqrt{3}$ phase) presenting an asymmetric and broad shoulder at a lower frequency (440–500 cm^{-1}) as reported in Fig. 3c (top panel).[148] DFT calculations rationalize the intense peak as the Raman active E_{2g} mode for the silicene superstructures.[150,151] Similar to graphene, the zone-center E_{2g} vibrational mode represents an in-plane displacement and is due to the bond stretching of all pairs of silicon atoms lying in six-atom rings with the frequency being strictly dependent on the Si–Si bond length. For freestanding silicene the E_{2g} mode is expected at a higher frequency ($\sim$570 cm^{-1}) because of the shorter bond length (2.28 Å, when calculated as an infinite sheet).[24] Hence, the softer E_{2g} mode of epitaxial silicene superstructures is related to the slightly longer Si–Si distance in the 4×4 phase (2.34–2.39 Å) and the $\sqrt{13} \times \sqrt{13}$ phase (2.31–2.36 Å) with respect to the cubic silicon. Conversely, the E_{2g} mode frequency of the $2\sqrt{3} \times 2\sqrt{3}$ silicene phase is blueshifted with respect to both the 4×4 and the $\sqrt{13} \times \sqrt{13}$, according to a shorter mean bond length (2.28–2.37 Å). Along with the purely

in-plane E_{2g} mode, additional out-of-plane modes contribute to the overall Raman spectrum of the Ag-supported silicene.[148,152] Basically, these consist of breathing-like displacements of the (planar and non-planar) hexagon rings constituting the silicene lattice.[148] An additional point of interest for the Raman spectroscopy of the Ag-supported silicene is the phase-dependent resonance behaviour (Fig. 3c, bottom). Resonant effects are usually measured in semiconductors as a function of the excitation wavelength. This is the case of the mixed $4 \times 4/\sqrt{13} \times \sqrt{13}$ silicene phase where the increasing Raman intensity is measured with increasing excitation wavelength. Conversely, no resonance is observed in the $2\sqrt{3} \times 2\sqrt{3}$ phase. This discrepancy is rationalized in terms of the different electronic band structures that are expected to take place with varying silicene phases, the 4×4 phase being qualified by a semiconducting bandgap and parabolic bands, whereas the $2\sqrt{3} \times 2\sqrt{3}$ one by Dirac bands with a semi-metallic character.[144,150,151] Although the resonant Raman scattering appears to be sensitive to the inner electronic structure of the Ag-supported silicene, this is not the case for photoemission and optical spectroscopies where silicene turns out to be strongly interacting with the substrate thus resulting in the suppression of the (expected) Dirac cones, the emergence of metallic hybrid bands arising from silicon p and silver d states,[62,65] and a metal-like carrier dynamics.[63]

The interpretation of the Raman spectrum of the encapsulated silicene is consistent with subsequent *in situ* investigations of the vibrational spectrum of the freshly grown (*i.e.* uncapped) Ag-supported silicene.[153,154] In these studies, not only is the asymmetric E_{2g} peak recognized but also additional features in the low frequency spectral range (below 220 cm^{-1}) are reported that were initially associated with the defect-induced D mode in analogy with graphene.[153] A closer insight into the latter aspect was gained by matching the experimental low-frequency datum with the phonon spectrum of the freestanding silicene[154] as well as by local inspection *via* tip-enhanced Raman spectroscopy (TERS).[155] Both approaches assign the low-frequency features to zone-centered modes A1 and A2 related to out-of-plane optical (ZO) phonons. Similar to the case of a single layer, the multilayer silicene (see Section 1.4) is also characterized by a sharp Raman mode that is blueshifted up to 526 cm^{-1} with respect to that of bulk silicon.[117] A similar shift is observed starting from the early growth stages of the $\sqrt{3} \times \sqrt{3}$ silicene phase that is a precursor for the multilayer silicene, in addition to a characteristic multi-peak profile in the low-frequency range associated with edge-induced scattering.[153]

Overall, though not as direct and explicative as the Raman spectrum of graphene, monitoring the main Raman-active mode on the encapsulated silicene proved to be a fast, non-destructive, and versatile tool to check the silicene status throughout a process sequence outside the vacuum ambient. Optical absorbance techniques are also emerging as an alternative option to probe the characteristic electronic DOS in silicene.[26,63]

3.3 Delamination transfer and device fabrication

Subsequent to the aforementioned encapsulated deposition of silicene, it is critical to keep the sandwich style Al_2O_3/silicene/Ag(111) film stack intact due to stability and portability concerns during operational approaches in the delamination transfer and device fabrication steps. Unlike graphene and other stable 2D materials, substrate etching based or wet transfer methods[156–158] cannot be readily applied to the case of silicene. The current SEDNE process entails mechanical delamination with a two-tape method to separate the Ag/silicene/Al_2O_3 stack from the mica substrate,[145] and then the application of the stack onto the device substrate (Approach-1 in Fig. 4a). The first tape picks up the Al_2O_3/silicene/Ag stack out from the bulk mica substrate, thanks to mica being a layered cleavable substrate. However, this delamination may not be perfect since some mica residues may remain in certain areas leading to a partial exposure of the Ag(111) surface. A second tape, such as the thermal releasing tape, then steps in to flip the Ag/silicene/Al_2O_3 film stack with the Al_2O_3 dielectric facing down before applying to a back-gate substrate. Both a blue tape with the least amount of adhesive and a thermal releasing tape (120–150 °C) are used in the delamination and transfer step. It is then feasible to obtain films, which are a few cm^2 in area with the delamination and transfer, with the uniformity of the films being monitored by Raman mapping. The SEDNE process sets a milestone in silicene device study, as a significant breakthrough to enable silicene transistors to make their debut, opening up exciting avenues of research and technology development. Below we envisage some perspectives to extend or upgrade SEDNE processing for the upcoming generation of silicene devices.

The delamination and transfer steps, as described above, significantly affect the device performance and yield. For the delamination step, it demands interface engineering between the supporting substrate and catalyst film. For the transfer step, it is critical to have seamless contact between the Al_2O_3 capping layer and device substrate. Both aspects call for innovative ideas to optimize silicene transistor design in future generation devices. In the transfer aspect, a promising process entails deposition of a thicker Al_2O_3 gate dielectric (Al_2O_3 capping in Fig. 4a) followed by a metal gate stack directly on top of the silicene stack. Subsequent to mica delamination, the whole stack can then be mounted onto a conductive host substrate (see the process flow in Fig. 4a) as a common back gate setup for electrical characteristics. Unlike the original SEDNE process which employs vacuum annealing steps to form a firm contact between the Al_2O_3 dielectric layer and back gate device substrate, the modified SEDNE approach leads to a seamless interface engineering between the silicene and gate dielectric plus a metal stack with simplified steps and reduced costs in time and energy.

In terms of delamination, it could also be possible to etch away the growth substrate, whilst the stack stays supported on the host substrate. Dry or wet etching with protected side-walls and back side of the stack could be explored. In this case, it is highly desirable to make use of a selective etchant, which attacks only mica, but does not affect the underlying silver layer. As mica etching could be challenging, it is worthwhile exploring other substrates that are lattice-matched with silver, and relatively easy to etch away selectively. One can also propose that the effort to remove the mica substrate (*e.g.* by etching) may

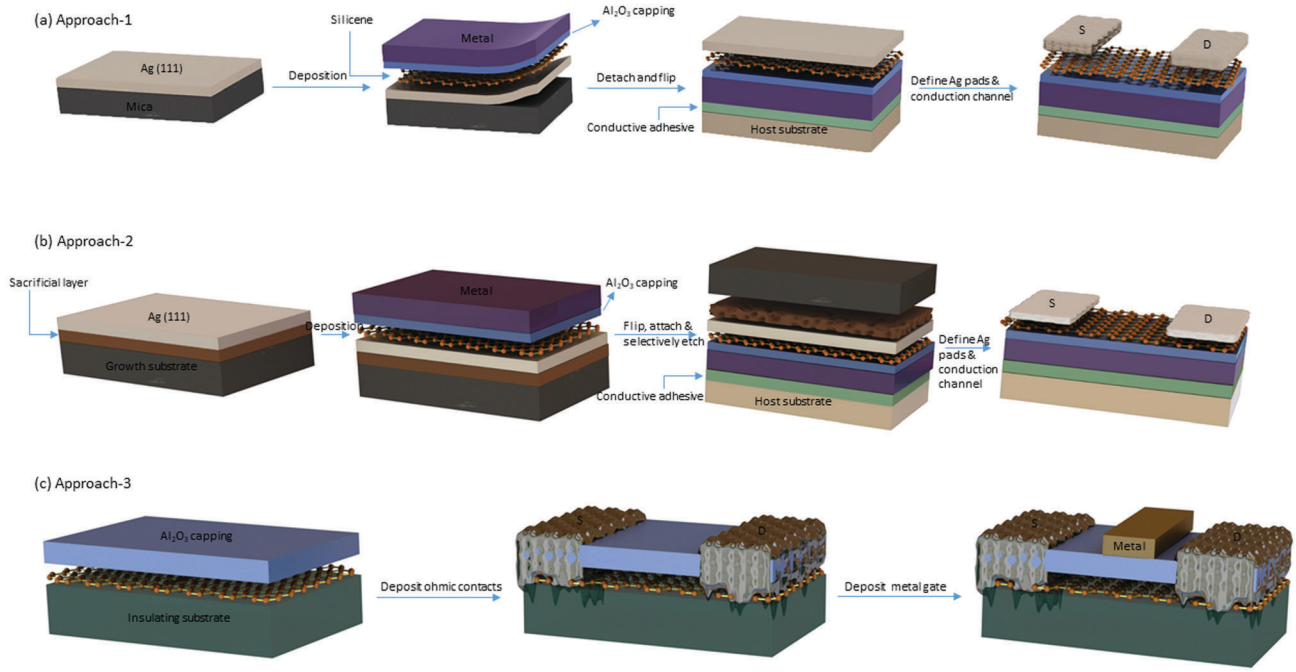

Fig. 4 Schematics demonstrating three different approaches for the fabrication of silicene devices. (a) Approach 1: Silicene Encapsulated Delamination with Native Electrode (SEDNE) process with additional Al_2O_3 and metal for back-gating devices. Building blocks of the process are: (i) deposit an epi-Ag(111) template on mica, (ii) grow silicene on silver, followed by deposition of an Al_2O_3 capping layer and a metal layer which acts as the gate, (iii) detach from mica, flip and attach on a highly doped host substrate with conductive adhesive, (iv) pattern Ag to define contacts and conduction channel. (b) Approach 2: hetero-integration of a sacrificial layer in between the growth substrate and Ag. Building blocks are: (i) integrate an easily removable and epitaxially compatible sacrificial layer in between the growth substrate and silver, (ii) grow silicene on silver, followed by deposition of an Al_2O_3 capping layer and a metal layer, (iii) flip stack and attach on a highly doped host substrate with a conductive adhesive, selectively etch sacrificial layer, leading to simultaneous detachment of the growth substrate, (iv) pattern silver to define contacts and conduction channel. (c) Approach 3: direct synthesis of silicene on insulating substrates. Building blocks are: (i) grow silicene on an insulating substrate followed by deposition of an Al_2O_3 capping layer on silicene, (ii) deposit and anneal (if required) ohmic contacts on Al_2O_3 to contact silicene, (iii) deposit a metal gate on top of Al_2O_3.

be facilitated by hetero-integration of a sacrificial layer, which is epitaxially compatible and easily removable, in between the substrate and silver (as shown in Approach-2 in Fig. 4b). Removal of the sacrificial layer through certain selective etching or other techniques would then simultaneously delaminate silicene from the growth substrate.

Selective etching of silver for patterning the source–drain contacts and the channel region is another crucial part of device fabrication and instant measurement. Silver electrode patterning is performed by means of two lithography steps: the first being electron beam lithography (EBL) on polymethyl methacrylate (PMMA) followed by wet-etching to define the source and drain contact pads, and the last being lithography and etching to open the silicene channel. For silver etching, rapid degradation of silicene was observed with commonly used etchants like nitric acid. A potassium iodide- and iodine-based etchant has been developed in-house for etching to form the Ag-free silicene channel.[145] While under-etching leaves the silver residue showing the metallic *I–V* response, over-etching instantly degrades silicene. It is therefore essential to perform calibration of the etching rate.

In the SEDNE process, a remaining challenge stems from the requirement of developing a post-fabrication passivating layer for silicene. This is a critical step to achieve a robust device enabling any thorough characterization of the electronic transport through silicene because of an extremely rapid ($\sim$2 minutes for monolayer) degradation under ambient conditions. It is beneficial to integrate a passivation layer with a high resistance to air and moisture and chemical inertness with robustness at cryogenic temperatures allowing for transport studies across a wide range of conditions. Possible candidates in this respect are non-interacting polymers or metal oxide dielectrics. Another approach to improve the durability of silicene devices is a symmetric dual-gate device structure, where silicene is sandwiched between two dielectric layers. Although this conceptual design was originally for better revealing charge transport behaviour under doping and gate control,[8] the sandwiched encapsulation is a good passivation strategy for experimental investigation on the silicene layer as well.

As the existing fabrication technique continues to evolve, it is important to note three key technical nodes: passivation, conceptual engineering of the device structure, and direct synthesis on the insulating substrate. As per the last aspect, processing of silicene-based devices would be much simplified if the silver template could be bypassed by use of insulating substrates. In this case, subsequent to growth, silicene could be capped with a thin layer of Al_2O_3 *in situ*, followed by deposition and annealing, if necessary, of the ohmic source, drain contacts

and deposition of gate metal all in the same *ex situ* process flow (Approach-3 in Fig. 4c). In this respect, having silicene synthesized on a device-friendly substrate can significantly facilitate the integration flow and strengthen the process reliability. A requirement for this purpose would rely on the use of non-interacting substrates where silicene can preserve its structural and electronic integrity during device fabrication stages. Reported cases of relevance are currently limited to a designer approach. For instance, transition metal dichalcogenides like MoS_2 and molybdenum telluride ($MoTe_2$) were proposed as templates for a vdW epitaxy of silicene (and other Xenes)[36] therein taking benefit from the intrinsic scalability (either lateral or vertical). Attempts to grow silicene and germanene in these substrates result in a metallic character. Nonetheless, MoS_2-supported silicene proved to bear transistor processing after Al_2O_3 encapsulation.[146] Alternatively, more recently Al_2O_3(0001), namely sapphire, was proposed as a candidate to accommodate silicene and germanene thus paving the way to the exploration of matter–light interaction otherwise inaccessible in metal substrates.[33] This would likely extend silicene's applications to the photonics field, as pointed out in Section 1.2.

3.4 A universal approach to Xene processing

(111)-Terminated silver or gold, that can be supported by mica substrates, are extensively used as templates for a number of epitaxial Xenes such as borophene, germanene, stanene, phosphorene, and antimonene (see Section 2.4). As such, the SEDNE process has merits to be recast as a universal path to process this kind of Xene with a silicene-like approach provided that portability and stability are ensured for each specific material (see Section 2.3). Fig. 5 depicts a main flow chart for the Universal Xene Encapsulation, Decoupling and Operation (UXEDO) process. Two key steps are as follows.

All-around encapsulation. It is necessary for air-sensitive Xenes, such as silicene and phosphorene, to have sandwiched or surrounded media to prevent oxidation or degradation. For instance, a conformal atomic layer deposition of Al_2O_3 could keep the investigated Xene intact for device fabrication. Otherwise, the side wall[159] or a one-side exposed surface[141] will be a leak source for hazardous molecules compromising the 2D materials. A complete encapsulation is inevitable to retain the pristine property.

Intact decoupling. The Xene needs to be transferred from the growth substrate to device substrates without sacrificing electrical properties through either the mechanical or chemical method. The key is to keep the relevant electronic states of Xene states approximately at the Fermi level, *i.e.* with minimum unintentional extrinsic doping induced. In practice, pre-defined structures (source, drain and gate pads along with the dielectrics) are desirable for achieving an intact decoupling of the Xene layer. Another common feature of this universal approach is to have pre-defined pads for optimized surface integration. This provides not only a cleaner interface by the direct contact of Xenes with dielectrics or metals without media residue, but also lower contact resistance for better device performance.

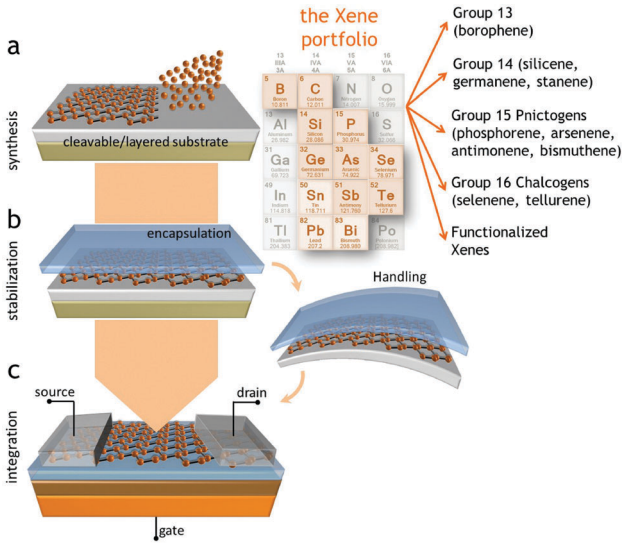

Fig. 5 Conceptual flow for the UXEDO process as a universal approach to treat epitaxial Xenes that are grown on cleavable or detachable substrates. Xenes of this kind are displayed in the extract from the periodic table around group 13–16 elements, functionalized Xenes are also listed as an engineered material option. Highlighted elements are those where reduction to the epitaxial Xene state has been shown. Process steps consists of: (a) epitaxial synthesis of the Xene on substrate and further functionalization if any, (b) stabilization *via* encapsulation and handling, (c) integration into an operational device (the field-effect transistor is taken as an example).

An additional merit of this universal Xene process is its versatility to several substrate types: either rigid (silicon, III–V compounds) or flexible substrates (plastic, fabrics, willow glass). This new universal approach addresses the major challenge of material preservation during the transfer and device fabrication for silicene, and is applicable to other air-sensitive Xenes such as germanene, stanene, phosphorene, and so on (Section 2.4).

4. Silicene-based technology applications

4.1 Silicene transistors

Silicene FET is an effective vehicle to understand the electronic properties of silicene and fulfil various electronic, sensing or even energy devices. After a briefing of simulation studies on silicene transistors, we will focus on the experimental performance and its correlation with bandgap engineering through device physics.

Some studies have summarized the simulation studies on dual-gated silicene FETs,[8,160] surface modified silicene FETs, silicene thin film FETs, silicene nanomesh FETs, silicene nanoribbon FETs *etc.* The gate modulation of these silicene FETs varies sharply from 4.2 to 4×10^8, while the bandgap has a narrow distribution of 160–680 meV, with more details available elsewhere.[161,162] Nevertheless, there are new developments in simulation on silicene transistors. Salimian *et al.* proposed a silicene nanotube FET by the transfer matrix method.[163] They investigated the effect of channel length,

chirality and diameter of a tube to the channel current, and concluded that the I_{max}/I_{min} ratio varies with chirality, diameter of silicene nanotubes, and perpendicular electric field, while the OFF current strongly depends on the characteristics of silicene nanotubes. Patel *et al.* reported that, in a dual-gate silicene FET, decreasing channel length degrades device parameters due to increased leakage whereas decreasing oxide thickness improves these parameters due to increased gate control over the silicene channel uniformly.[164] The evaluation of silicene FET requires considering characteristic parameters, such as mobility, gate modulation (I_{max}/I_{min} ratio), subthreshold swing, transconductance *etc.*, which all connect to one key phrase: bandgap engineering, either through an external electrical field or through chemical or physical surface modification.

The experimental investigation on silicene transistors was falling behind theoretical or simulation study due to air stability and fabrication portability issues as previously discussed in Section 3.3. Electrostatic transfer and output measurements, such as the drain current (I_d) response to gate voltage (V_g), on monolayer silicene (Ag-free) transistors under ambient conditions (Fig. 6a) revealed device behaviour similar to graphene, corroborating theoretical expectations on ambipolar Dirac charge transport.[150] This work also supports DFT calculations of the p–d hybridization of Si–Ag stabilized silicene grown on Ag(111).[167] In addition, we discovered that material characteristics, such as the number of layers, could play a role in the stability and electrical characteristics of silicene transistors. According to the electrostatic measurement data, single-layer silicene could yield a field-effect mobility of $\mu \sim 100$ cm^2 V^{-1} s^{-1} at a residual carrier density of $\sim 5 \times 10^9$ cm^{-2} with a gate modulation of around 11×, whereas multilayer silicene showed a broader I_d–V_g curve and a similar mobility of $\sim$200 cm^2 V^{-1} s^{-1} at a residual carrier density of 2×10^{12} cm^{-2} (Fig. 6b). Multilayer silicene devices exhibited a notably longer lifetime up to 48 h compared to 2 minutes for the monolayer counterparts.[117] The field-effect mobility (μ) and residual carrier density (n_o) data provide abundant information about the band structure of silicene. Though pristine free-standing silicene is predicted to offer an intrinsic mobility of $\sim$1000 cm^2 V^{-1} s^{-1},[168] the substrate effect on silicene's acoustic phonon energies and electron–phonon coupling is likely perturbed negatively in our experimental studies and results in a much lower mobility value than calculated. We recall here that the thermally generated n_o of a Dirac semiconductor with a zero bandgap inherently depends on the Fermi velocity (v_F), with $n_o \propto (1/v_F^2)$.[169] Given that the v_F of silicene is comparable to that of graphene[48,168] the most plausible scenario to understand silicene's low n_o necessitates a small bandgap opening. In the limit of a weak perturbation to the Dirac dispersion of Ag-free silicene, the small bandgap that yields $n_o \sim 8 \times 10^9$ cm^{-2} is calculated to be $\sim$210 meV,[145] falling into the theoretically calculated range.[162]

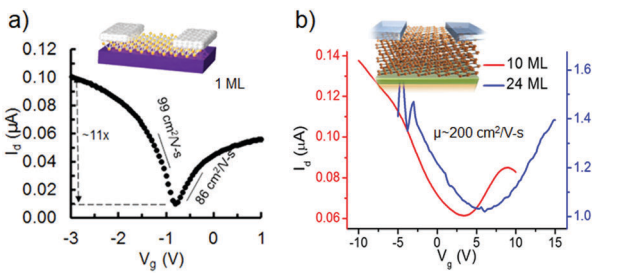

Fig. 6 Electrical characterization of silicene devices: (a) transfer characteristic curve of monolayer silicene with $\sim$11× gate modulation, exhibiting a gate control over a dozen samples with extracted low-field carrier mobilities of 99 and 86 cm^2 V^{-1} s^{-1} for electrons and holes, respectively, (b) multilayer silicene with a broader ambipolar I_d–V_g curve and mobility $\sim$200 cm^2 V^{-1} s^{-1} (stable up to 48 h). Panel (a) is adapted from ref. 145 with permission from Springer Nature, copyright 2015. Panel (b) is adapted from ref. 117 with permission from the American Chemical Society, copyright 2017.

Silicene exhibits a higher SOC than graphene and the bandgap opening is relatively more practical.[170] The latter one is a unique property of Xenes like silicene and other akin materials such as exfoliated phosphorene, enabling potential applications based on their transistors that graphene cannot afford (Table 1). Core research on silicene transistors is about bandgap engineering. There are four approaches to engineer the bandgap of silicene: chemical modification, topography (*e.g.* nanoribbons), coupling to a substrate and external electric field.[171] The above-mentioned experimental work on back-gate silicene transistors demonstrated that coupling to a substrate and applying an external vertical electric field could effectively tune or engineer the band structure. It also provides transferable knowledge to explore the other two approaches.

4.2 Silicene for topology-based electronics

As discussed in Section 2, silicene is predicted to be a 2D-TI that hosts the QSH effect.[5,172] 2D TIs are characterized by bulk insulating states with gapless helical edge states, which are protected against backscattering by time-reversal symmetry.[28,173] Transport through the helical edge states is ideally dissipationless even in the presence of (non-magnetic) defects, meaning that silicene could be a very promising material for applications in low-energy electronics. With recent advances in research on topological states of matter, the QSH state has emerged as a potential candidate for building novel quantum mechanical switches, the so-called topological insulator field-effect transistors (TI-FETs) (Fig. 7c), which can be turned ON/OFF by a topological phase transition, as opposed to the conventional charge accumulation/depletion.[12] The topological phase can be switched (Fig. 7a and b) between a non-trivial, ballistic QSH edge state (ON state) and a trivial insulating bulk state (OFF state) with the application of a gate voltage (strain). The critical field required ($E_c = 2\lambda_{SO}/\delta$, where $2\lambda_{SO}$ is the SOC induced bandgap), for topological phase transition in silicene is approximately 0.05 eV nm^{-1}, almost an order of magnitude less than the breakdown field of conventional solid-state-dielectrics ($E_{SiO_2} \sim 0.7$ eV nm^{-1}). Nonetheless, higher (lower) SOC results in room (low) temperature operation with a comparatively high (low) critical electric field for realization of topological phase transition. Hence, silicene, with its moderate

Table 1 Comparison of key device parameters in Xenes

Xene sheets	Band gap (eV)	I_{max}/I_{min}	Field-effect mobility ($cm^2\ V^{-1}\ s^{-1}$)	Residual carrier density (cm^{-2})
Graphene[165]	0	5–10	18 000[a]	10^{11-12}
Silicene[117,145]	0–0.2	10–12	100–200	10^{9-12}
Phosphorene[b] [166]	0.3–2	10^{2-4}	200–1560	—

[a] Measured at room temperature on SiO_2. [b] Exfoliated from black phosphorus.

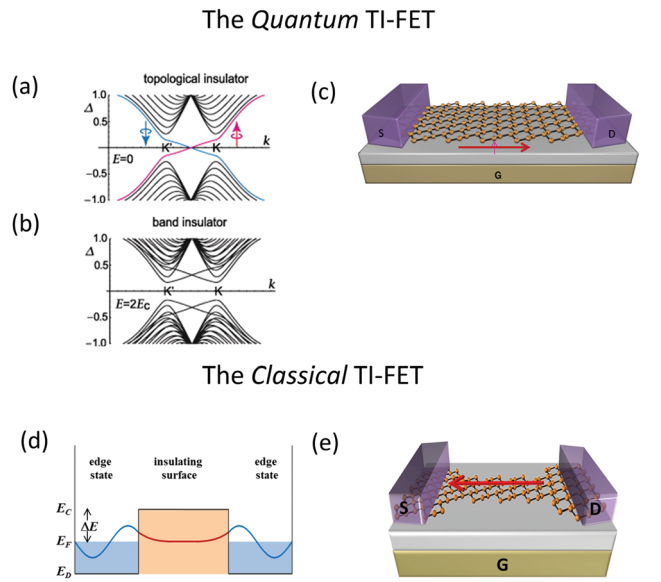

Fig. 7 Topology as a technology driver for 2D silicon. (a) Non-trivial topological edge states crossing the gap at pristine silicene (ON/topological insulator). There are two edge states since a nanoribbon has two edges (red and blue lines for the left and right edges). (b) Edge states disappear with the application of an out-of-plane electric field greater than the critical field (OFF/band insulator). Panel (a and b) are adapted from ref. 181 with permission from IOP publishing, copyright 2012. (c) Quantum TI-FET driven by an out-of-plane electric field. (d) A simplified double quantum well model (along the transverse direction) for understanding the nanoribbon width and energy barrier dependence of the tunnelling and overlap of the wave-function of edge electrons. (e) Sketch of a classical TI-FET device structure predicated on inter-edge scattering in the 2D nanoribbon owing to the nanoribbon width and controllable by the field-effect on E_F.

SOC (1.55 meV)[5] that limits its operation in relatively low temperature, is still a potential candidate for gate tunable TI-FETs due to its critical field value allowing the topological phase transition.

A different approach for realization of classical TI-FETs (Fig. 7e) which is free from the critical field operation temperature trade-off of quantum TI-FETs, has been proposed.[174] This scheme is based on engineering inter-edge elastic scattering of the edges of 2D TI materials for modulating the conductivity of the channel and hence puts a limitation on the width of the silicene nanoribbon just to make sure the edge-scattering is sufficient to play a role in device operation. According to the model, the conductivity decreases ($\sigma \sim e^{\Delta E/kT}$, ΔE is the energy barrier between the conduction band and Fermi energy) with the electric-field due to the reduction in the energy barrier facilitated by phonon-mediated scattering of edge electrons into bulk states. This is quite opposite to the operation of conventional thermionic FETs, where the field-effect enhances carrier density (lowers barrier) and hence enhances conductivity ($\sigma \sim e^{-\Delta E/kT}$). The device physics can be better understood by using the double quantum well model (Fig. 7d) where the quantum wells are represented as edge states in an insulating bulk. In this model, the basic parameter is the field-dependent tunnelling length scale given by

$$l_t = \frac{\hbar}{\sqrt{2m^*\Delta E}} \approx \frac{2\ \text{Å}}{\sqrt{\left(\frac{m^*}{m_o}\right)\Delta E}},$$

where ΔE is in eV, and m^* and m_o are the effective mass of bulk electrons and the electron rest mass, respectively. This amounts to $\sim$10 nm for silicene and to ensure sufficient inter-edge interactions, nanoribbon silicene TI-FETs should have ribbon widths within an order of magnitude of l_t ($\lesssim$100 nm).

4.3 Perspectives for silicene-based junctions

Besides homogeneous silicene sheets or nanotubes, there is increasing research interest in silicene based junctions or heterostructures that hold great promise for exotic electronic,[160,164] magnetic, and thermal applications.[175–177] Zhou *et al.* theoretically investigated the spin transport in a silicene channel with a Fe(111)/silicene stack injector.[176] The partial DOS of the iron layer in this combination shows that spin-down states dominate above the Fermi level, resulting in a negligible spin-up current and high spin injection efficiency. Thus, they present the Fe(111)/silicene heterostructure as a good candidate for achieving efficient spin injection devices. Interestingly, thermo-spin is another option for silicene-junction based spintronic devices. Zhai *et al.* proposed a heterojunction of silicene (or germanene) intercalated between two ferromagnetic dielectric layers, and such a configuration with a proximity-induced asymmetric magnetic field could yield an attractive phenomenon named the valley-locked spin-dependent Seebeck effect (VL-SSE) driven by a thermal gradient.[175] The VL-SSE operates in a way that the charge carriers from only one valley get thermally excited, having the opposite spin polarization counter-propagating along the direction of the thermal gradient, whereas the nearly zero carrier is excited from the other insulating valley due to the relatively wide bandgap. It is worth noting that thermal conductivity is a critical parameter still lacking in research for the silicene-based junction or heterostructure applications. Zhang *et al.* utilized a multiscale modelling approach (molecular dynamics plus finite element analysis) to investigate the heat dissipation in 2D transistors based on phosphorene and silicene.[177] They found that the heat dissipation ability of 2D transistors improves by increasing

the thermal conductivities of the channel and substrate, *i.e.* forming a phosphorene/silicene heterostructure.

Energy storage is another field of interest for applications involving silicene-based junctions. In this respect, multilayer silicene was recently proposed as an anode for Li-ion batteries instead of conventionally used graphite.[178] This direction is driven by the exceptionally high specific capacity of silicon (4200 mA h g^{-1}) against graphite ($\approx$371 mA h g^{-1}). Similar to graphite, the multilayer silicene would enable intercalation/deintercalation of lithium atoms during charge/discharge of the cell despite an expected capacity scaling down to $\approx$954 mA h g^{-1}. This functionality is basically supported by the high versatility of silicene to recast in multiple lithiated configurations.[179] For this purpose, multilayer silicene grown on Ag(111) (see Section 1.4) can be readily processed *via* encapsulation free decoupling as described in Section 2.4 for further integration into a battery-functional junction. However, thorough investigation of the oxidation mechanism in multilayer silicene is required to assess the environmental stability in such a configuration.

Overall, silicene-based junctions have plenty of perspective applications not limited to the aforementioned thermal or spintronic (magnetic-spin or thermos-spin) or energy cases, as silicene is an ideal channel material with prominent characteristics, such as a tunable band gap and compatibility with the ubiquitous semiconductor industry.

5. Conclusions

Since the rise of epitaxial silicene in 2012, not only has the literature about it been tremendously expanding, but also new research forefronts on silicene-like Xenes have been consequently triggered. As a result, silicene and its derivatives could potentially offer an intriguing platform for both fundamental research and device applications. For the former aspect, Xenes share the common virtue of buckled elemental atomic sheets, which enclose a rich variety of fundamental properties of matter and particle physics. Concomitantly, as for the latter aspect, previous challenges regarding the accessibility, stability, and portability of silicene have been addressed, with promising experimental device study supporting theoretical prediction on the Dirac cone existing in its electronic band structure. As witnessed by the recent experimental research progress in epitaxial growth, Raman characterization, interface engineering, and device fabrication, silicene and its derivatives are one step closer to integration of the QSH effect, topological bits, flexible electronics, and energy devices, to name a few. Nevertheless, there is still a lack of experimental study on these exotic device ideas that may inspire or foster on-going work on the impact of silicene on societal challenges. Specifically, several material and processing correlated issues are yet to be resolved, such as interface matching between Xenes and dielectrics or metal contacts on device substrates, and post-fabrication passivation. Inspiringly, recent synthetic (superlattice and number of layer control) and processing (sandwich encapsulation) advances are encouraging towards further adventures involving exotic quantum and topological phenomena in silicene and similar Xenes for potentially innovative device concepts revolutionizing current semiconductor technology.

Conflicts of interest

There are no conflicts to declare.

Acknowledgements

A. M. acknowledges funding support from H2020 ERC CoG 2017 grant No. 772261 ''XFab''. A. M. and C. G. acknowledge funding support from CNR grant Laboratori Congiunti ''SFET'', and Fondazione CARIPLO – Regione Lombardia for the project ''Crystel'', grant No. 2016-0978. D. A. acknowledges support from the Army Research Office (ARO), the Presidential Early Career Award for Engineers and Scientists (PECASE), and the Gordon and Betty Moore Foundation. L. T. acknowledges support from the Young 1000-Talent Award #12 (2016), the National Science Foundation of China (51602051), and the Fundamental Research Funds for the Central Universities (2242017R30008).

Notes and references

1 M. I. Katsnelson, *Mater. Today*, 2007, **10**, 20–27.
2 J. E. Moore, *Nature*, 2010, **464**, 194–198.
3 K. Takeda and K. Shiraishi, *Phys. Rev. B: Condens. Matter Mater. Phys.*, 1994, **50**, 14916–14922.
4 K. S. Novoselov, A. K. Geim, S. V. Morozov, D. Jiang, Y. Zhang, S. V. Dubonos, I. V. Grigorieva and A. A. Firsov, *Science*, 2004, **306**, 666–669.
5 C.-C. Liu, W. Feng and Y. Yao, *Phys. Rev. Lett.*, 2011, **107**, 076802.
6 S. Rachel and M. Ezawa, *Phys. Rev. B: Condens. Matter Mater. Phys.*, 2014, **89**, 195303.
7 C. Xu, G. Luo, Q. Liu, J. Zheng, Z. Zhang, S. Nagase, Z. Gao and J. Lu, *Nanoscale*, 2012, **4**, 3111.
8 Z. Ni, Q. Liu, K. Tang, J. Zheng, J. Zhou, R. Qin, Z. Gao, D. Yu and J. Lu, *Nano Lett.*, 2012, **12**, 113–118.
9 N. D. Drummond, V. Zólyomi and V. I. Fal'ko, *Phys. Rev. B: Condens. Matter Mater. Phys.*, 2012, **85**, 075423.
10 H. Bao, W. Liao, J. Guo, H. Zhao and G. Zhou, *Laser Phys. Lett.*, 2015, **12**, 095902.
11 H. M. Le, T.-T. Pham, T. S. Dinh, Y. Kawazoe and D. Nguyen-Manh, *J. Phys.: Condens. Matter*, 2016, **28**, 135301.
12 A. Molle, J. Goldberger, M. Houssa, Y. Xu, S. C. Zhang and D. Akinwande, *Nat. Mater.*, 2017, **16**, 163–169.
13 N. M. Johnson and M. D. Moyer, *Appl. Phys. Lett.*, 1985, **46**, 787–789.
14 N. M. Johnson, D. K. Biegelsen and M. D. Moyer, *Appl. Phys. Lett.*, 1982, **40**, 882–884.

15 S. Trivedi, A. Srivastava and R. Kurchania, *J. Comput. Theor. Nanosci.*, 2014, **11**, 781–788.
16 M. M. Atalla, E. Tannenbaum and E. J. Scheibner, *Bell Syst. Tech. J.*, 1959, **38**, 749–783.
17 H. N. Khan, D. A. Hounshell and E. R. H. Fuchs, *Nat. Electron.*, 2018, **1**, 14–21.
18 M. Bruel, *MRS Bull.*, 1998, **23**, 35–39.
19 K. Uchida and S. Takagi, *Appl. Phys. Lett.*, 2003, **82**, 2916–2918.
20 Z.-G. Shao, X.-S. Ye, L. Yang and C.-L. Wang, *J. Appl. Phys.*, 2013, **114**, 093712.
21 S. Cahangirov, M. Topsakal, E. Aktürk, H. Şahin and S. Ciraci, *Phys. Rev. Lett.*, 2009, **102**, 236804.
22 D. Jose and A. Datta, *J. Phys. Chem. C*, 2012, **116**, 24639–24648.
23 S. Ryu and Y. Hatsugai, *Phys. Rev. Lett.*, 2002, **89**, 077002.
24 M. Houssa, G. Pourtois, V. V. Afanas'ev and A. Stesmans, *Appl. Phys. Lett.*, 2010, **97**, 112106.
25 G. G. Guzmán-Verri and L. C. Lew Yan Voon, *Phys. Rev. B*, 2007, **76**, 075131.
26 L. Matthes, O. Pulci and F. Bechstedt, *New J. Phys.*, 2014, **16**, 105007.
27 M. Ezawa, *EPL*, 2013, **104**, 27006.
28 C. L. Kane and E. J. Mele, *Phys. Rev. Lett.*, 2005, **95**, 226801.
29 M. Ezawa, *Phys. Rev. Lett.*, 2012, **109**, 055502.
30 C. J. Tabert and E. J. Nicol, *Phys. Rev. Lett.*, 2013, **110**, 197402.
31 M. Ezawa, *J. Phys. Soc. Jpn.*, 2015, **84**, 121003.
32 C. Grazianetti, E. Cinquanta and A. Molle, *2D Mater.*, 2016, **3**, 012001.
33 M. X. Chen, Z. Zhong and M. Weinert, *Phys. Rev. B*, 2016, **94**, 075409.
34 A. Bhattacharya, S. Bhattacharya and G. P. Das, *Appl. Phys. Lett.*, 2013, **103**, 123113.
35 S. Kokott, P. Pflugradt, L. Matthes and F. Bechstedt, *J. Phys.: Condens. Matter*, 2014, **26**, 185002.
36 E. Scalise, M. Houssa, E. Cinquanta, C. Grazianetti, B. van den Broek, G. Pourtois, A. Stesmans, M. Fanciulli and A. Molle, *2D Mater.*, 2014, **1**, 11010.
37 H. Liu, J. Gao and J. Zhao, *J. Phys. Chem. C*, 2013, **117**, 10353–10359.
38 M. Houssa, B. van den Broek, E. Scalise, G. Pourtois, V. V. Afanas'ev and A. Stesmans, *Phys. Chem. Chem. Phys.*, 2013, **15**, 3702.
39 P. Pflugradt, L. Matthes and F. Bechstedt, *New J. Phys.*, 2014, **16**, 075004.
40 P. De Padova, P. Perfetti, B. Olivieri, C. Quaresima, C. Ottaviani and G. Le Lay, *J. Phys.: Condens. Matter*, 2012, **24**, 223001.
41 S. Sheng, R. Ma, J. Wu, W. Li, L. Kong, X. Cong, D. Cao, W. Hu, J. Gou, J.-W. Luo, P. Cheng, P.-H. Tan, Y. Jiang, L. Chen and K. Wu, *Nano Lett.*, 2018, **18**, 2937–2942.
42 A. J. Mannix, X.-F. Zhou, B. Kiraly, J. D. Wood, D. Alducin, B. D. Myers, X. Liu, B. L. Fisher, U. Santiago, J. R. Guest, M. J. Yacaman, A. Ponce, A. R. Oganov, M. C. Hersam and N. P. Guisinger, *Science*, 2015, **350**, 1513–1516.
43 B. Feng, J. Zhang, Q. Zhong, W. Li, S. Li, H. Li, P. Cheng, S. Meng, L. Chen and K. Wu, *Nat. Chem.*, 2016, **8**, 563–568.
44 C.-H. Lin, A. Huang, W. W. Pai, W.-C. Chen, T.-Y. Chen, T.-R. Chang, R. Yukawa, C.-M. Cheng, C.-Y. Mou, I. Matsuda, T.-C. Chiang, H.-T. Jeng and S.-J. Tang, *Phys. Rev. Mater.*, 2018, **2**, 024003.
45 J. Yuhara, Y. Fujii, K. Nishino, N. Isobe, M. Nakatake, L. Xian, A. Rubio and G. Le Lay, *2D Mater.*, 2018, **5**, 025002.
46 Y. Shao, Z.-L. Liu, C. Cheng, X. Wu, H. Liu, C. Liu, J.-O. Wang, S.-Y. Zhu, Y.-Q. Wang, D.-X. Shi, K. Ibrahim, J.-T. Sun, Y.-L. Wang and H.-J. Gao, *Nano Lett.*, 2018, **18**, 2133–2139.
47 H.-C. Hsu, Y.-H. Lu, T.-L. Su, W.-C. Lin and T.-Y. Fu, *Semicond. Sci. Technol.*, 2018, **33**, 075004.
48 P. Vogt, P. De Padova, C. Quaresima, J. Avila, E. Frantzeskakis, M. C. Asensio, A. Resta, B. Ealet and G. Le Lay, *Phys. Rev. Lett.*, 2012, **108**, 155501.
49 C.-L. Lin, R. Arafune, K. Kawahara, N. Tsukahara, E. Minamitani, Y. Kim, N. Takagi and M. Kawai, *Appl. Phys. Express*, 2012, **5**, 045802.
50 L. Meng, Y. L. Wang, L. Z. Zhang, S. X. Du, R. T. Wu, L. F. Li, Y. Zhang, G. Li, H. T. Zhou, W. A. Hofer and H.-J. J. Gao, *Nano Lett.*, 2013, **13**, 685–690.
51 D. Chiappe, E. Scalise, E. Cinquanta, C. Grazianetti, B. van den Broek, M. Fanciulli, M. Houssa and A. Molle, *Adv. Mater.*, 2014, **26**, 2096–2101.
52 T. Aizawa, S. Suehara and S. Otani, *J. Phys. Chem. C*, 2014, **118**, 23049–23057.
53 L. Huang, Y.-F. Zhang, Y.-Y. Zhang, W. Xu, Y. Que, E. Li, J.-B. Pan, Y.-L. Wang, Y. Liu, S.-X. Du, S. T. Pantelides and H.-J. Gao, *Nano Lett.*, 2017, **17**, 1161–1166.
54 M. De Crescenzi, I. Berbezier, M. Scarselli, P. Castrucci, M. Abbarchi, A. Ronda, F. Jardali, J. Park and H. Vach, *ACS Nano*, 2016, **10**, 11163–11171.
55 D. Chiappe, C. Grazianetti, G. Tallarida, M. Fanciulli and A. Molle, *Adv. Mater.*, 2012, **24**, 5088–5093.
56 B. J. Feng, Z. J. Ding, S. Meng, Y. G. Yao, X. Y. He, P. Cheng, L. Chen and K. H. Wu, *Nano Lett.*, 2012, **12**, 3507–3511.
57 H. Jamgotchian, Y. Colignon, N. Hamzaoui, B. Ealet, J. Y. Hoarau, B. Aufray and J. P. Bibérian, *J. Phys.: Condens. Matter*, 2012, **24**, 172001.
58 R. Arafune, C.-L. Lin, K. Kawahara, N. Tsukahara, E. Minamitani, Y. Kim, N. Takagi and M. Kawai, *Surf. Sci.*, 2013, **608**, 297–300.
59 C. Grazianetti and A. Molle, in *GraphITA*, ed. V. Morandi and L. Ottaviano, Springer, Cham, 2017, pp. 137–152.
60 Z.-L. Liu, M.-X. Wang, J.-P. Xu, J.-F. Ge, G. Le Lay, P. Vogt, D. Qian, C.-L. Gao, C. Liu and J.-F. Jia, *New J. Phys.*, 2014, **16**, 075006.
61 C. Grazianetti, D. Chiappe, E. Cinquanta, M. Fanciulli and A. Molle, *J. Phys.: Condens. Matter*, 2015, **27**, 255005.
62 D. Tsoutsou, E. Xenogiannopoulou, E. Golias, P. Tsipas and A. Dimoulas, *Appl. Phys. Lett.*, 2013, **103**, 231604.
63 E. Cinquanta, G. Fratesi, S. dal Conte, C. Grazianetti, F. Scotognella, S. Stagira, C. Vozzi, G. Onida and A. Molle, *Phys. Rev. B: Condens. Matter Mater. Phys.*, 2015, **92**, 165427.
64 J. Avila, P. De Padova, S. Cho, I. Colambo, S. Lorcy, C. Quaresima, P. Vogt, a. Resta, G. Le Lay and M. C. Asensio, *J. Phys.: Condens. Matter*, 2013, **25**, 262001.

65 S. K. Mahatha, P. Moras, V. Bellini, P. M. Sheverdyaeva, C. Struzzi, L. Petaccia and C. Carbone, *Phys. Rev. B: Condens. Matter Mater. Phys.*, 2014, **89**, 201416.
66 L. Chen, C.-C. Liu, B. Feng, X. He, P. Cheng, Z. Ding, S. Meng, Y. Yao and K. Wu, *Phys. Rev. Lett.*, 2012, **109**, 056804.
67 Y. Feng, D. Liu, B. Feng, X. Liu, L. Zhao, Z. Xie, Y. Liu, A. Liang, C. Hu, Y. Hu, S. He, G. Liu, J. Zhang, C. Chen, Z. Xu, L. Chen, K. Wu, Y.-T. Liu, H. Lin, Z.-Q. Huang, C.-H. Hsu, F.-C. Chuang, A. Bansil and X. J. Zhou, *Proc. Natl. Acad. Sci. U. S. A.*, 2016, **113**, 14656–14661.
68 P. Gori, O. Pulci, F. Ronci, S. Colonna and F. Bechstedt, *J. Appl. Phys.*, 2013, **114**, 113710.
69 Z.-X. Guo, S. Furuya, J. Iwata and A. Oshiyama, *Phys. Rev. B: Condens. Matter Mater. Phys.*, 2013, **87**, 235435.
70 Y.-P. Wang and H.-P. Cheng, *Phys. Rev. B: Condens. Matter Mater. Phys.*, 2013, **87**, 245430.
71 C. L. Lin, R. Arafune, K. Kawahara, M. Kanno, N. Tsukahara, E. Minamitani, Y. Kim, M. Kawai and N. Takagi, *Phys. Rev. Lett.*, 2013, **110**, 76801.
72 S. Cahangirov, M. Audiffred, P. Tang, A. Iacomino, W. Duan, G. Merino and A. Rubio, *Phys. Rev. B: Condens. Matter Mater. Phys.*, 2013, **88**, 035432.
73 M. Satta, S. Colonna, R. Flammini, A. Cricenti and F. Ronci, *Phys. Rev. Lett.*, 2015, **115**, 026102.
74 C. Vacacela Gomez, M. Pisarra, M. Gravina, P. Riccardi and A. Sindona, *Phys. Rev. B*, 2017, **95**, 085419.
75 R. Friedlein and Y. Yamada-Takamura, *J. Phys.: Condens. Matter*, 2015, **27**, 203201.
76 H. Okamoto, Y. Sugiyama and H. Nakano, *Chem. – Eur. J.*, 2011, **17**, 9864–9887.
77 E. Noguchi, K. Sugawara, R. Yaokawa, T. Hitosugi, H. Nakano and T. Takahashi, *Adv. Mater.*, 2015, **27**, 856–860.
78 R. Yaokawa, T. Ohsuna, T. Morishita, Y. Hayasaka, M. J. S. Spencer and H. Nakano, *Nat. Commun.*, 2016, **7**, 10657.
79 S. M. Pratik, A. Nijamudheen and A. Datta, *Chem. – Eur. J.*, 2015, **21**, 18454–18460.
80 S. Yamanaka, *Dalton Trans.*, 2010, **39**, 1901–1915.
81 A. M. Tokmachev, D. V. Averyanov, I. A. Karateev, O. E. Parfenov, A. L. Vasiliev, S. N. Yakunin and V. G. Storchak, *Nanoscale*, 2016, **8**, 16229–16235.
82 A. M. Tokmachev, D. V. Averyanov, I. A. Karateev, O. E. Parfenov, O. A. Kondratev, A. N. Taldenkov and V. G. Storchak, *Adv. Funct. Mater.*, 2017, **27**, 1606603.
83 A. M. Tokmachev, D. V. Averyanov, O. E. Parfenov, A. N. Taldenkov, I. A. Karateev, I. S. Sokolov, O. A. Kondratev and V. G. Storchak, *Nat. Commun.*, 2018, **9**, 1672.
84 S. Botti, J. A. Flores-Livas, M. Amsler, S. Goedecker and M. A. L. Marques, *Phys. Rev. B: Condens. Matter Mater. Phys.*, 2012, **86**, 121204.
85 Y. He, H. Li, Y. Sui, J. Qi, Y. Wang, Z. Chen, J. Dong and X. Li, *Sci. Rep.*, 2015, **5**, 14792.
86 F. Gimbert, C.-C. Lee, R. Friedlein, A. Fleurence, Y. Yamada-Takamura and T. Ozaki, *Phys. Rev. B: Condens. Matter Mater. Phys.*, 2014, **90**, 165423.
87 H. I. T. Hauge, M. A. Verheijen, S. Conesa-Boj, T. Etzelstorfer, M. Watzinger, D. Kriegner, I. Zardo, C. Fasolato, F. Capitani, P. Postorino, S. Kölling, A. Li, S. Assali, J. Stangl and E. P. A. M. Bakkers, *Nano Lett.*, 2015, **15**, 5855–5860.
88 D. Y. Kim, S. Stefanoski, O. O. Kurakevych and T. A. Strobel, *Nat. Mater.*, 2014, **14**, 169–173.
89 S. W. Kim, J. Lee, J. H. Sung, D. Seo, I. Kim, M.-H. Jo, B. W. Kwon, W. K. Choi and H.-J. Choi, *ACS Nano*, 2014, **8**, 6556–6562.
90 S. Lee, K. Kim, K. P. Dhakal, H. Kim, W. S. Yun, J. Lee, H. Cheong and J.-H. Ahn, *Nano Lett.*, 2017, **17**, 7744–7750.
91 J. Lang, B. Ding, S. Zhang, H. Su, B. Ge, L. Qi, H. Gao, X. Li, Q. Li and H. Wu, *Adv. Mater.*, 2017, **29**, 1701777.
92 V. Q. Bui, T.-T. Pham, H.-V. S. Nguyen and H. M. Le, *J. Phys. Chem. C*, 2013, **117**, 23364–23371.
93 N. Gao, G. Y. Lu, Z. Wen and Q. Jiang, *J. Mater. Chem. C*, 2017, **5**, 627–633.
94 B. Huang, H. J. Xiang and S.-H. Wei, *Phys. Rev. Lett.*, 2013, **111**, 145502.
95 H. Sahin and F. M. Peeters, *Phys. Rev. B: Condens. Matter Mater. Phys.*, 2013, **87**, 085423.
96 J. Sivek, H. Sahin, B. Partoens and F. M. Peeters, *Phys. Rev. B: Condens. Matter Mater. Phys.*, 2013, **87**, 085444.
97 T. H. Osborn, A. A. Farajian, O. V. Pupysheva, R. S. Aga and L. C. Lew Yan Voon, *Chem. Phys. Lett.*, 2011, **511**, 101–105.
98 Y. Du, J. Zhuang, H. Liu, X. Xu, S. Eilers, K. Wu, P. Cheng, J. Zhao, X. Pi, K. W. See, G. Peleckis, X. Wang and S. X. Dou, *ACS Nano*, 2014, **8**, 10019–10025.
99 R. Wang, X. Pi, Z. Ni, Y. Liu, S. Lin, M. Xu and D. Yang, *Sci. Rep.*, 2013, **3**, 3507.
100 T. Morishita and M. J. S. Spencer, *Sci. Rep.*, 2015, **5**, 17570.
101 V. O. Özçelik, S. Cahangirov and S. Ciraci, *Phys. Rev. Lett.*, 2014, **112**, 246803.
102 Y. Y. Du, J. Zhuang, J. Wang, Z. Li, H. Liu, J. Zhao, X. Xu, H. Feng, L. Chen, K. Wu, X. Wang and S. X. Dou, *Sci. Adv.*, 2016, **2**, e1600067.
103 J. Qiu, H. Fu, Y. Xu, Q. Zhou, S. Meng, H. Li, L. Chen and K. Wu, *ACS Nano*, 2015, **9**, 11192–11199.
104 W. Wang, W. Olovsson and R. I. G. Uhrberg, *Phys. Rev. B*, 2016, **93**, 081406.
105 J. Qiu, H. Fu, Y. Xu, A. I. Oreshkin, T. Shao, H. Li, S. Meng, L. Chen and K. Wu, *Phys. Rev. Lett.*, 2015, **114**, 126101.
106 S. Cahangirov, V. O. Özçelik, A. Rubio and S. Ciraci, *Phys. Rev. B: Condens. Matter Mater. Phys.*, 2014, **90**, 085426.
107 S. Cahangirov, V. O. Özçelik, L. Xian, J. Avila, S. Cho, M. C. Asensio, S. Ciraci and A. Rubio, *Phys. Rev. B: Condens. Matter Mater. Phys.*, 2014, **90**, 035448.
108 P. Vogt, P. Capiod, M. Berthe, A. Resta, P. De Padova, T. Bruhn, G. Le Lay and B. Grandidier, *Appl. Phys. Lett.*, 2014, **104**, 021602.
109 F. Zhu, W. Chen, Y. Xu, C. Gao, D. Guan, C. Liu, D. Qian, S.-C. Zhang and J. Jia, *Nat. Mater.*, 2015, **14**, 1020–1025.
110 P. De Padova, A. Generosi, B. Paci, C. Ottaviani, C. Quaresima, B. Olivieri, E. Salomon, T. Angot and G. Le Lay, *2D Mater.*, 2016, **3**, 031011.
111 H. Fu, L. Chen, J. Chen, J. Qiu, Z. J. Ding, J. Zhang, K. H. Wu, H. Li and S. Meng, *Nanoscale*, 2015, **7**, 15880–15885.

112 P. De Padova, P. Vogt, A. Resta, J. Avila, I. Razado-Colambo, C. Quaresima, C. Ottaviani, B. Olivieri, T. Bruhn, T. Hirahara, T. Shirai, S. Hasegawa, M. Carmen Asensio and G. Le Lay, *Appl. Phys. Lett.*, 2013, **102**, 163106.
113 Z. Li, J. Zhuang, L. Chen, Z. Ni, C. Liu, L. Wang, X. Xu, J. Wang, X. Pi, X. Wang, Y. Du, K. Wu and S. X. Dou, *ACS Cent. Sci.*, 2016, **2**, 517–521.
114 A. J. Mannix, B. Kiraly, B. L. Fisher, M. C. Hersam and N. P. Guisinger, *ACS Nano*, 2014, **8**, 7538–7547.
115 S. K. Mahatha, P. Moras, P. M. Sheverdyaeva, R. Flammini, K. Horn and C. Carbone, *Phys. Rev. B: Condens. Matter Mater. Phys.*, 2015, **92**, 245127.
116 A. Curcella, R. Bernard, Y. Borensztein, M. Lazzeri, A. Resta, Y. Garreau and G. Prévot, *2D Mater.*, 2017, **4**, 025067.
117 C. Grazianetti, E. Cinquanta, L. Tao, P. De Padova, C. Quaresima, C. Ottaviani, D. Akinwande and A. Molle, *ACS Nano*, 2017, **11**, 3376–3382.
118 H.-S. Tsai, C.-H. Hsiao, C.-W. Chen, H. Ouyang and J.-H. Liang, *Nanoscale*, 2016, **8**, 9488–9492.
119 V. Kochat, A. Samanta, Y. Zhang, S. Bhowmick, P. Manimunda, S. A. S. Asif, A. S. Stender, R. Vajtai, A. K. Singh, C. S. Tiwary and P. M. Ajayan, *Sci. Adv.*, 2018, **4**, e1701373.
120 M. Pumera and Z. Sofer, *Adv. Mater.*, 2017, **29**, 1605299.
121 S. Zhang, Z. Yan, Y. Li, Z. Chen and H. Zeng, *Angew. Chem., Int. Ed.*, 2015, **54**, 3112–3115.
122 L. Xian, A. Pérez Paz, E. Bianco, P. M. Ajayan and A. Rubio, *2D Mater.*, 2017, **4**, 041003.
123 M. Derivaz, D. Dentel, R. Stephan, M. C. Hanf, A. Mehdaoui, P. Sonnet and C. Pirri, *Nano Lett.*, 2015, **15**, 2510–2516.
124 J. Gou, Q. Zhong, S. Sheng, W. Li, P. Cheng, H. Li, L. Chen and K. Wu, *2D Mater.*, 2016, **3**, 045005.
125 M. E. Dávila, L. Xian, S. Cahangirov, A. Rubio and G. Le Lay, *New J. Phys.*, 2014, **16**, 095002.
126 L. Li, S. Lu, J. Pan, Z. Qin, Y. Wang, Y. Wang, G. Cao, S. Du and H.-J. Gao, *Adv. Mater.*, 2014, **26**, 4820–4824.
127 Z. Qin, J. Pan, S. Lu, Y. Shao, Y. Wang, S. Du, H.-J. Gao and G. Cao, *Adv. Mater.*, 2017, **29**, 1606046.
128 L. Zhang, P. Bampoulis, A. N. Rudenko, Q. Yao, A. van Houselt, B. Poelsema, M. I. Katsnelson and H. J. W. Zandvliet, *Phys. Rev. Lett.*, 2016, **116**, 256804.
129 F. d'Acapito, S. Torrengo, E. Xenogiannopoulou, P. Tsipas, J. Marquez Velasco, D. Tsoutsou and A. Dimoulas, *J. Phys.: Condens. Matter*, 2016, **28**, 045002.
130 C.-Z. Xu, Y.-H. Chan, P. Chen, X. Wang, D. Flötotto, J. A. Hlevyack, G. Bian, S.-K. Mo, M.-Y. Chou and T.-C. Chiang, *Phys. Rev. B*, 2018, **97**, 035122.
131 Z. Zhu and D. Tománek, *Phys. Rev. Lett.*, 2014, **112**, 176802.
132 J. L. Zhang, S. Zhao, C. Han, Z. Wang, S. Zhong, S. Sun, R. Guo, X. Zhou, C. D. Gu, K. Di Yuan, Z. Li and W. Chen, *Nano Lett.*, 2016, **16**, 4903–4908.
133 T. Hirahara, G. Bihlmayer, Y. Sakamoto, M. Yamada, H. Miyazaki, S. Kimura, S. Blügel and S. Hasegawa, *Phys. Rev. Lett.*, 2011, **107**, 166801.
134 F. Reis, G. Li, L. Dudy, M. Bauernfeind, S. Glass, W. Hanke, R. Thomale, J. Schäfer and R. Claessen, *Science*, 2017, **357**, 287–290.
135 X. Wu, Y. Shao, H. Liu, Z. Feng, Y.-L. Wang, J.-T. Sun, C. Liu, J.-O. Wang, Z.-L. Liu, S.-Y. Zhu, Y.-Q. Wang, S.-X. Du, Y.-G. Shi, K. Ibrahim and H.-J. Gao, *Adv. Mater.*, 2017, **29**, 1605407.
136 M. Fortin-Deschênes, O. Waller, T. O. Menteş, A. Locatelli, S. Mukherjee, F. Genuzio, P. L. Levesque, A. Hébert, R. Martel and O. Moutanabbir, *Nano Lett.*, 2017, **17**, 4970–4975.
137 J. Chen, Y. Dai, Y. Ma, X. Dai, W. Ho and M. Xie, *Nanoscale*, 2017, **9**, 15945–15948.
138 X. Huang, J. Guan, Z. Lin, B. Liu, S. Xing, W. Wang and J. Guo, *Nano Lett.*, 2017, **17**, 4619–4623.
139 J. Qin, G. Qiu, J. Jian, H. Zhou, L. Yang, A. Charnas, D. Y. Zemlyanov, C.-Y. Xu, X. Xu, W. Wu, H. Wang and P. D. Ye, *ACS Nano*, 2017, **11**, 10222–10229.
140 Y. Du, G. Qiu, Y. Wang, M. Si, X. Xu, W. Wu and P. D. Ye, *Nano Lett.*, 2017, **17**, 3965–3973.
141 A. Molle, C. Grazianetti, D. Chiappe, E. Cinquanta, E. Cianci, G. Tallarida and M. Fanciulli, *Adv. Funct. Mater.*, 2013, **23**, 4340–4344.
142 X. Xu, J. Zhuang, Y. Du, H. Feng, N. Zhang, C. Liu, T. Lei, J. Wang, M. Spencer, T. Morishita, X. Wang and S. X. Dou, *Sci. Rep.*, 2015, **4**, 7543.
143 H. Van Bui, F. B. Wiggers, R. Friedlein, Y. Yamada-Takamura, A. Y. Kovalgin and M. P. de Jong, *J. Chem. Phys.*, 2015, **142**, 064702.
144 M. Houssa, B. Van Den Broek, E. Scalise, B. Ealet, G. Pourtois, D. Chiappe, E. Cinquanta, C. Grazianetti, M. Fanciulli, A. Molle, V. V. Afanas'Ev and A. Stesmans, *Appl. Surf. Sci.*, 2014, **291**, 98–103.
145 L. Tao, E. Cinquanta, D. Chiappe, C. Grazianetti, M. Fanciulli, M. Dubey, A. Molle and D. Akinwande, *Nat. Nanotechnol.*, 2015, **10**, 227–231.
146 A. Molle, A. Lamperti, D. Rotta, M. Fanciulli, E. Cinquanta and C. Grazianetti, *Adv. Mater. Interfaces*, 2016, **3**, 1500619.
147 R. Friedlein, H. Van Bui, F. B. Wiggers, Y. Yamada-Takamura, A. Y. Kovalgin and M. P. de Jong, *J. Chem. Phys.*, 2014, **140**, 204705.
148 E. Cinquanta, E. Scalise, D. Chiappe, C. Grazianetti, B. Van Den Broek, M. Houssa, M. Fanciulli and A. Molle, *J. Phys. Chem. C*, 2013, **117**, 16719–16724.
149 A. C. Ferrari and D. M. Basko, *Nat. Nanotechnol.*, 2013, **8**, 235–246.
150 E. Scalise, E. Cinquanta, M. Houssa, B. van den Broek, D. Chiappe, C. Grazianetti, G. Pourtois, B. Ealet, A. Molle, M. Fanciulli, V. V. Afanas'ev and A. Stesmans, *Appl. Surf. Sci.*, 2014, **291**, 113–117.
151 E. Scalise, M. Houssa, G. Pourtois, B. van den Broek, V. Afanas'ev and A. Stesmans, *Nano Res.*, 2013, **6**, 19–28.
152 E. Scalise, Vibrational Properties of Silicene and Germanene, *Vibrational Properties of Defective Oxides and 2D Nanolattices*, Springer Theses, Springer, Cham, 2014.
153 J. Zhuang, X. Xu, Y. Du, K. Wu, L. Chen, W. Hao, J. Wang, W. K. Yeoh, X. Wang and S. X. Dou, *Phys. Rev. B: Condens. Matter Mater. Phys.*, 2015, **91**, 161409.

154 D. Solonenko, O. D. Gordan, G. Le Lay, H. Şahin, S. Cahangirov, D. R. T. Zahn and P. Vogt, *2D Mater.*, 2016, **4**, 015008.
155 S. Sheng, J. Wu, X. Cong, W. Li, J. Gou, Q. Zhong, P. Cheng, P. Tan, L. Chen and K. Wu, *Phys. Rev. Lett.*, 2017, **119**, 196803.
156 X. Li, W. Cai, J. An, S. Kim, J. Nah, D. Yang, R. Piner, A. Velamakanni, I. Jung, E. Tutuc, S. K. Banerjee, L. Colombo and R. S. Ruoff, *Science*, 2009, **324**, 1312–1314.
157 X. Li, Y. Zhu, W. Cai, M. Borysiak, B. Han, D. Chen, R. D. Piner, L. Colombo and R. S. Ruoff, *Nano Lett.*, 2009, **9**, 4359–4363.
158 J. W. Suk, A. Kitt, C. W. Magnuson, Y. Hao, S. Ahmed, J. An, A. K. Swan, B. B. Goldberg and R. S. Ruoff, *ACS Nano*, 2011, **5**, 6916–6924.
159 J.-S. Kim, Y. Liu, W. Zhu, S. Kim, D. Wu, L. Tao, A. Dodabalapur, K. Lai and D. Akinwande, *Sci. Rep.*, 2015, **5**, 8989.
160 Z. Zhuo, X. Wu and J. Yang, *Nanoscale*, 2018, **10**, 1265–1271.
161 R.-G. Quhe, Y.-Y. Wang and J. Lü, *Chin. Phys. B*, 2015, **24**, 088105.
162 J. Zhao, H. Liu, Z. Yu, R. Quhe, S. Zhou, Y. Wang, C. C. Liu, H. Zhong, N. Han, J. Lu, Y. Yao and K. Wu, *Prog. Mater. Sci.*, 2016, **83**, 24–151.
163 F. Salimian and D. Dideban, *ECS J. Solid State Sci. Technol.*, 2018, **7**, M1–M5.
164 N. Patel and S. Choudhary, *Superlattices Microstruct.*, 2017, **110**, 155–161.
165 A. Reina, X. Jia, J. Ho, D. Nezich, H. Son, V. Bulovic, M. S. Dresselhaus and J. Kong, *Nano Lett.*, 2009, **9**, 30–35.
166 L. Tao, W. Zhu, J.-S. Kim and D. Akinwande, 2015 45th European Solid State Device Research Conference (ESSDERC), IEEE, 2015, pp. 168–171.
167 J. Gao, G. Zhang and Y.-W. Zhang, *Sci. Rep.*, 2016, **6**, 29107.
168 X. Li, J. T. Mullen, Z. Jin, K. M. Borysenko, M. Buongiorno Nardelli and K. W. Kim, *Phys. Rev. B: Condens. Matter Mater. Phys.*, 2013, **87**, 1–9.
169 P. J. Dobson, *Contemp. Phys.*, 2012, **53**, 379–380.
170 M. Vali, D. Dideban and N. Moezi, *J. Comput. Electron.*, 2016, **15**, 138–143.
171 H. J. W. Zandvliet, *Nano Today*, 2014, **9**, 691–694.
172 M. Tahir, A. Manchon, K. Sabeeh and U. Schwingenschlögl, *Appl. Phys. Lett.*, 2013, **102**, 162412.
173 X.-L. Qi, T. L. Hughes and S.-C. Zhang, *Phys. Rev. B: Condens. Matter Mater. Phys.*, 2010, **81**, 134508.
174 W. G. Vandenberghe and M. V. Fischetti, *J. Appl. Phys.*, 2014, **116**, 173707.
175 X. Zhai, Y.-T. Wang, R. Wen, S.-X. Wang, Y. Tian, X. Zhou, W. Chen and Z. Yang, *Phys. Rev. B*, 2018, **97**, 085410.
176 J. Zhou, A. Bournel, Y. Wang, X. Lin, Y. Zhang and W. Zhao, *Appl. Phys. Lett.*, 2017, **111**, 182408.
177 H. Zhang, H. Wang, S. Xiong, H. Han, S. Volz and Y. Ni, *J. Phys. Chem. C*, 2018, **122**, 2641–2647.
178 J. Zhuang, X. Xu, G. Peleckis, W. Hao, S. X. Dou and Y. Du, *Adv. Mater.*, 2017, **29**, 1606716.
179 G. A. Tritsaris, E. Kaxiras, S. Meng and E. Wang, *Nano Lett.*, 2013, **13**, 2258–2263.
180 H. Enriquez, S. Vizzini, A. Kara, B. Lalmi and H. Oughaddou, *J. Phys.: Condens. Matter*, 2012, **24**, 314211.
181 M. Ezawa, *New J. Phys.*, 2012, **14**, 033003.